Hydrologic behavior of model slopes with synthetic water repellent soils

Shuang Zheng[1], Sérgio D.N. Lourenço[1*], Peter J. Cleall[2], Ting Fong May Chui[1], Angel K.Y. Ng[3], Stuart W. Millis[3]

[1] Department of Civil Engineering, The University of Hong Kong, Hong Kong S.A.R., China

[2] School of Engineering, Cardiff University, United Kingdom

[3] Ove Arup & Partners (Hong Kong) Ltd., Hong Kong S.A.R, China

* Corresponding author

Abstract

In the natural environment, soil water repellency decreases infiltration, increases runoff, and increases erosion in slopes. In the built environment, soil water repellency offers the opportunity to develop granular materials with controllable wettability for slope stabilization. In this paper, the influence of soil water repellency on the hydrological response of slopes is investigated. Twenty-four flume tests were carried out in model slopes under artificial rainfall; soils with various wettability levels were tested, including wettable (Contact angle, CA <90°), subcritical water repellent (CA ~90°) and water repellent (CA >90°). Various rainfall intensities (30 mm/h and 70 mm/h), slope angles (20° and 40°) and relative compactions (70% and 90%) were applied to model the response of natural and man-made slopes to rainfall. To quantitatively assess the hydrological response, a number of measurements were made: runoff rate, effective rainfall rate, time to ponding, time to steady state, runoff acceleration, total water storage and wetting front rate. Overall, an increase in soil water repellency reduces infiltration and shortens the time for runoff generation, with the effects amplified for high rainfall intensity. Comparatively, the slope angle and relative compaction had only minor contribution to the slope hydrology. The subcritical water repellent soils sustained infiltration for longer than both the wettable and water repellent soils, which presents an added advantage if they are to be used in the built environment as barriers. This study revealed substantial impacts of man-made or synthetically induced soil water repellency on the hydrological behavior of model slopes in controlled conditions. The results shed light on our understanding of hydrological processes in environments where the occurrence of natural soil water repellency is likely, such as slopes subjected to wildfires and in agricultural and forested slopes.

Keywords: Soil wettability, synthetic water repellent soil, hydrological behavior, flume test

1. Introduction

Wildfire-induced water repellent soil (soil that exhibit low affinity for water) is widely known for altering the hydrological responses and vadose zone processes of hillslopes, such as formation of unstable wetting front and fingered flow (preferential flow), restricted soil water movement and redistribution, decreased infiltration rate and promoted surface runoff (Doerr et al., 2006; Ritsema and Dekker, 2000; DeBano, 2000). By impeding infiltration into soil matrix, enhancing the overland flow and increasing the erodibility of soils, the likelihood of post-wildfire debris flows and consequent flash floods is increased (Fox et al., 2007; Cannon et al., 2008; Kean et al., 2012; Robichaud et al., 2016).

Soil wettability, a measure of the affinity of soils for water, is closely related to the stability of slopes. The strong correlation between post-wildfire debris flows and the formation or enhancement of soil water repellency has been extensively reported. Soil water repellency reduces the infiltration rate and increases the erodibility thereby resulting in increased overland flow and erosion. On the other hand, for wettable natural soils (soils that exhibit high affinity for water) the infiltration rate is relatively high and rainwater is able to infiltrate through the slope and form a saturated zone above any impermeable layer, leading to a rapid rise in the pore water pressure and a decrease of the effective stress and soil strength eventually triggering failure (Wang and Sassa, 2001; Tohari et al., 2007) whilst other factors known to influence slope stability of wettable soils such as rainfall intensity (RI), slope angle and relative compaction (for man-made slopes) have been widely reported and known for decades, little is known about their effects with regard to water repellent soils in slopes.

The soil-hydraulic properties of burned and unburned soils have been measured and compared). Ebel and Moody (2017) reported that the mean value of sorptivity (a measure of the liquid movement in a porous material by capillarity) for unburned soils was seven times greater than that of burned soils, whereas the field saturated hydraulic conductivity was not significantly decreased in burned soils compared with unaffected soils. However, Fox et al. (2007) and Robichaud (2000) conducted laboratory and field experiments and observed reduced saturated hydraulic conductivity on water repellent soils. The effects of water repellency on other soil properties have also been investigated, such as water retention (Czachor et al., 2010; Lourenço et al., 2015a), splash erodibility (Ahn et al., 2013), water drop impact (Hamlett et al., 2013), and permeability and compressibility for saturated wax-coated soils (Bardet et al., 2014), water entry pressure and friction angle (Lee et al., 2015) and small-strain shear modulus (Choi et al., 2016). However, although the association between wildfire-induced water repellency and enhanced hydrological response in the form of runoff and erosion is generally accepted, it is challenging to separate the influence of water repellency from other impacts such as a reduction in the vegetation cover and surface sealing with pore clogging.

Although soil water repellency is generally linked to limited or no infiltration, debris flows and erosion, its ability to impede water infiltration into soil has drawn the interest of engineers due to its waterproof capabilities. Synthetic water repellent soils have been used for water harvesting in arid areas (Meyers and Frasier, 1969). DeBano (1981) proposed the installation of a water repellent layer in the pavement base to prevent water permeation and protect the pavement from freezing and thawing. The potential use of synthetic water repellent soils as alternative landfill cover has also been proposed by Dell'Avanzi et al. (2010). Lourenço et al. (2015c) conducted a series of flume tests to model the response of slopes under rainfall, by manipulating the level of wettability from wettable to water repellent to explore the application of water repellent soils in slope engineering. Bardet et al. (2014) applied wax-coated sands on horseracing tracks and sports fields to avoid the degradation of the soil properties under rainfall.

To date, the use of synthetic water repellent soils has only considered a fully water repellent condition where no infiltration occurs (impermeable to water). However, wettability is controllable with the possibility of adjusting its condition so that some water infiltrates (i.e. semi-permeable to water). This could represent an added advantage for applications where vegetation is required to grow or where erosion is expected. Therefore, since extreme wettability conditions can cause slope instability in the form of landslides or erosion, the optimal conditions that reduce or inhibit slope instability need to be established so that synthetic water repellent soils could be deployed on sloping ground. This paper explores the influence of four factors assumed to alter the hydrologic response of the slope, namely: level of water repellency, slope angle, soil relative density and rainfall intensity.

The aim of the paper is to investigate the effect of synthetically induced soil water repellency on the hydrological response of slopes with a view to establish the conditions that minimize slope instability, either through excessive runoff, erosion or slope failure. In particular, soils with three wettability levels (wettable, subcritical water repellent and water repellent) were tested through a series of flume tests in model slopes at defined relative compactions, slope angles and rainfall intensities. The wettability levels are based on the contact angle (CA). If the water drop is placed on a water repellent surface, it does not infiltrate instantaneously. The angle that develops at the three-phase line is called the CA, which depends on the relation between the interfacial energies of the three involved surfaces (solid, liquid and vapor). The CA of a wettable soil and water repellent soil is $<90°$ and $>90°$ respectively, and a subcritical water repellent soil has a CA ~90°. A subcritical water-repellent condition reduces infiltration and is generally regarded as a wettability boundary between wettable and water repellent soil (Czachor et al., 2010). The specific objectives of the study are: 1) to identify the infiltration modes and estimate the infiltration rates for the different wettability levels; 2) to assess the longevity of the wettability levels (for the sub-critical and water repellent soils); 3) to assess the effects of rainfall intensity, slope angle and relative compaction on the hydrological responses within each wettability level; and 4) to determine the optimal conditions under which the runoff, erosion or slope failure is diminished or inhibited.

2. Materials and Methods

2.1. Soil description

The soil selected in this study is completely decomposed granite (CDG), collected from Happy Valley, Hong Kong, which is widespread locally and commonly used as an engineering soil and fill material (Lumb, 1965). The mineralogy of CDG was analyzed using X-ray diffraction (XRD) (Philips, PW1710 Automated Powder Diffractometer, Almelo, The Netherlands), and the major mineral compositions are quartz and kaolinite. Particle size distribution, compaction behavior and organic matter content were obtained for the natural CDG (Table 1). The percentage of sand and fines was 49.47% and 34.47% respectively. The high proportion of fines agrees with the large proportion of kaolinite from the XRD results. The CDG is classified as a well-graded silty sand based on the particle size distribution (Figure 1). The maximum dry density and optimum water content with the light Proctor test were 1.57 Mg/m^3 and 23%, respectively. Loss on ignition (LOI) analysis was conducted to determine the organic matter content (BS 1377-3:1990). Sub-samples were heated at 450°C for 1 hour. The organic content was 1.95%. The soil was air-dried and sieved (6.30 mm mesh with the coarser material discarded) for further use.

2.2. Soil water repellency assessment

Two measuring techniques were adopted in this study to assess the level of water repellency of different soil samples: the sessile drop method (SDM) and water drop penetration time (WDPT).

2.2.1. Sessile Drop Method

The SDM is a direct method to measure the CA of water drop on a soil sample surface. This method was improved by Bachmann et al. (2000) and the procedure is as follows: the soil is sprinkled on a double-sided adhesive tape fixed on a glass slide, the excess particles are removed to ensure a monolayer of particles is fixed and any motion of the particles is prevented. Placing the slide on a goniometer's stage and dispensing a droplet of deionized water (10μL) on the sample. CA measurements are then performed with a goniometer (DSA 25, KRÜSS GmbH, Germany), by analyzing the shape of the droplet on the soil surface. The analyzing technique proposed by Saulick et al. (2017) was adopted. By applying this semi-automatic technique, the standard deviation of measurements on a granular surface was improved by 33%, comparing to the conventional analyzing technique.

2.2.2. Water Drop Penetration Time test

WDPT is an index test that evaluates the persistency of water repellency of a soil sample. The test involves dispensing a drop of deionized water (50μL) on the surface of prepared soil sample and recording the time for the water drop to completely infiltrate (Doerr, 1998). For wettable soils the water drop should penetrate immediately, and for water repellent soils, the stronger the water repellency the longer the time it takes to fully infiltrate. Based on the penetration time, the water repellency of soils can be classified into different categories (Table 2).

2.3. Water repellent soil treatment

Inorganic soils are considered to be wettable as the surface energy of commonly composing minerals (silica and calcite) is higher than that of water (Lourenço et al., 2015b). The occurrence of soil water repellency results from the presence of water repellent coatings around the soil particles. Naturally occurring soil water repellency is usually caused by plant surface wax and certain fungi species (Bisdom et al., 1993; DeBano, 2000). Therefore, a variety of water repellent substances similar to those in nature has been used to induce water repellency, such as stearic acid (Leelamanie and Karube, 2009), oleic acid (Wijewardana et al., 2015) and tung oil (Zhang et al., 2016).

Natural soil water repellency is not time-stable, with changes in the wettability status possible with time. To achieve persistent and stable soil water repellency, dimethyldichlorosilane (DMDCS) has been used as a hydrophobizing agent to form a water repellent coating on soil samples (Bachmann et al., 2000; Ng and Lourenço, 2016). The mechanism of the treatment is based on silanization. By reaction between DMDCS and residual water, polydimethylsiloxane (PDMS) is formed and bonded to the soil particle surface along with the formation of HCl gas as a by-product.

The level of water repellency depends on the concentration of DMDCS and soil type. Bachmann et al. (2000) used 7.5 mL DMDCS per kg of sand and 50 mL DMDCS per kg of silt to attain a CA~90° (which is a quantification of water repellency). Ng and Lourenço (2016) found that the maximum CA can be induced by 3% and 0.005% DMDCS by soil mass for alluvium and Leighton Buzzard sand, respectively. The concentration of DMDCS to attain high water repellency in CDG was found to be 3% DMDCS by soil mass to achieve a CA ~115° (Figure 2). After the treatment, a significant increase in the level of soil water repellency was observed. As shown in Figure 3, the CAs of treated soils increased in the first 3 days and then slightly fluctuated, regardless of the DMDCS concentration. This was assumed to be due to a continuing reaction with water vapor to release the hydrochloric acid. To allow water repellency to establish in the soils and for consistency among the tests, the soil was treated and equilibrated at ambient air conditions for 3 days before using.

2.4. Flume tests

Flume tests at various scales have been widely conducted to study the initiation and dynamics of debris flows under artificial rainfall (Eckersley, 1990; Iverson and LaHusen, 1993; Wang and Sassa, 2001; Lourenço et al., 2015c). To investigate the influence of wettability change on hydrological responses of soil, 24 flume tests were carried out in a perspex-sided flume. The dimensions of the physical model were 80 cm long, 40 cm wide and 10 cm high. Sandpaper (Simax LPE-22-4) was glued on the bottom of the flume to provide friction and prevent the model from sliding at the flume-soil interface. As this research focuses on the hydrological response of soils of variable wettability under rainfall and to minimize potential mechanical effects, a baffle was installed at the toe of the slope to prevent sliding of the soil mass. The absence of a retaining element at the toe of the slope would enhance erosion in the toe area. This was the case in flume tests with a trapezoidal shape (Lourenço et al., 2006) where toe erosion and back-sliding controlled failure. Artificial rainfall was generated by a nozzle, controlled by a flowmeter, to ensure constant RI during tests. Four capacitance moisture sensors (EC-5, Decagon Devices, US) were installed at two different depths (3 and 8 cm respectively) to track the volumetric water content change. The sensors measure the volumetric water content of the soil by measuring the dielectric permittivity, and a soil-specific calibration was performed using the technique recommended by Cobos and Chambers (2010). A video camera (HERO4 Silver, GoPro, US) was positioned parallel to the side to capture the movement of the wetting front and the slope failure process. The resolution of the camera is 3840 × 2160 pixels with a sampling frequency of 15 frames per second. Figure 4 shows the configuration of the flume and instrumentation.

2.4.1. Model preparation and test procedure

Testing was conducted on dry water repellent CDG since water repellency develops in drier soils. The CDG was initially air-dried and treated to the desired CA, no water was added and no oven-drying was conducted prior or after treatment as the temperature is known to influence soil water repellency. The model was compacted in a horizontal orientation into 10 layers with a thickness of 1 cm. For each layer, the mass of soil was calculated and the dumping height and compaction energy controlled to attain a given relative compaction. Four moisture sensors were buried during the compaction, two on the second layer (depth: 8 cm) and the other two on the seventh layer from the bottom (depth: 3 cm). In order to prevent infiltration on the flume sides, a side wall intercept was glued on both sides of the flume to divert the rainfall out of the flume (Figure 4a). This portion of the rainfall was collected together with the surface runoff and excluded in the data analysis. After compaction, the flume was inclined to the desired slope angle.

At the onset of each test, the artificial rainfall was applied at a determined intensity. The advance of the wetting front, which was sensitive to the wettability change, was monitored by the camera. This information was validated by the moisture sensors, which can trace the spatial evolution of wetting at 1-minute intervals. Runoff and the soil discharge were collected by a storage container at the end of the flume at 5-minute intervals. Runoff is equivalent to the difference between rainfall intensity and effective rainfall rate. When the steady state is reached, the runoff discharge equals to rainfall intensity and remains unchanged, that means the effective rainfall is zero. Within this context, the term runoff does not necessarily imply overland flow. As will be later presented, most observed runoff occurs at the sub-surface, with water flowing within the top mm’s of the soil profile parallel to the surface.

2.4.2. Testing programme

Twenty-four flume tests were conducted (Table 3) under different slope inclinations, relative compactions, rainfall intensities and wettability. As this study originates in Hong Kong, the slope angles, relative compactions and rainfall intensities were selected to represent Hong

Kong natural and man-made slopes. Slope inclinations were from 20° to 40°, where 20° is on the small end of slope angle for local man-made slopes (Sun, 1999) and 40° is the largest that can be obtained using this flume. The majority of fill slopes in Hong Kong are within this range. The two relative compactions selected were 70% and 90%, with a corresponding dry density of 1.10 Mg/m^3 and 1.41 Mg/m^3, respectively. For the relative compaction, 70% corresponds to an uncompacted soil, whilst 90% is the maximum relative compaction that can be obtained with the soil in a dry state.

As for RI, black and amber rainstorm signals of Hong Kong's rainstorm warning system (Li and Lai, 2004) were selected with the intensities of 70 mm/h and 30 mm/h respectively. The Hong Kong Intensity-Duration-Frequency (IDF) relationships recommended in the stormwater drainage manual (Drainage Services Department, 2013) was adopted to determine the relation between rainfall duration, rainfall intensity and the return period. A rainfall duration of 120 minutes was adopted for all tests, since preliminary testing indicated that the steady state condition was achieved for the duration of 90-120 minutes. Therefore, a rainfall duration of 120 minutes under a RI of 70 mm/h and 30 mm/h correspond to a return period of 10 years and 2 years, respectively. There was a small difference in the RI among the tests at 20° and 40° slope angles, as the nozzle was fixed in vertical orientation and the area of apparent horizontal plan changes with slope angle. The RI was determined by measuring the volume of rainfall that accumulated in cups at various locations. The actual RI was 69.8±6.1 mm/h and 30.4±1.8 mm/h for a slope angle of 40°, and 74.4±4.6 mm/h and 34.2±3.3 mm/h for a slope angle of 20°.

Three water repellency levels were selected by treating the CDG at increasing concentrations of DMDCS. The criteria were based on the CA and WDPT attained. For a wettable condition the CA and WDPT should be as low as possible. For a sub-critical water repellent condition the CA should be ~90° and the WDPT >0 seconds. For a water repellent condition the CA and WDPT should be as high as possible. Therefore, the CDG in an untreated state delivered a CA ~55° and a WDPT = 0 seconds corresponding to the wettable condition. Sub-critical water repellent conditions were achieved at 1.8% DMDCS concentration (CA ~92°, WDPT rising). Water repellent conditions were achieved for 3% DMDCS concentration (CA ~115°, WDPT extreme) (Figure 2).

2.5. Data analysis

The raw data generated in each test includes: 1) volumetric water content at 4 different locations; 2) runoff discharge at 5-minute intervals and 3) photographs of infiltration modes. A series of variables were defined to analyze the data (Figure 5):

- Runoff rate (q, mm/h): Volume of water runoff collected at each 5-minute interval.

- Effective rainfall rate (i, mm/h): Difference between RI (r, mm/h) and runoff rate (q) at each 5-minute interval (Stoof et al., 2014). Both the runoff rate (q) and effective rainfall rate (i) were presented in time series. The expression for infiltrate rate is as follows:

$$i = r - q \quad (1)$$

- Time to ponding (t_p, min): Determined from visual inspection of ponding at the slope surface (Diskin and Nazimov, 1996) and a corresponding growth in the runoff rate (q).

- Time to steady state (t_{ss}, min): Time at which the runoff rate (q) is equal to the rainfall intensity. The time to steady state (t_{ss}) follows the time to ponding (t_p) and corresponds the time at which all rainfall becomes runoff (i.e. no more water storage).

- Runoff acceleration (a_q, mm/h^2): The temporal change in the runoff rate (q) (not the temporal change in water flow velocity) from time to ponding (t_p) to time to steady state (t_{ss}). It represents how fast the runoff developed before steady state was reached and can be calculated by

$$a_q = \frac{\Delta q}{t_{ss} - t_p} \quad (2)$$

- Total water storage (S, mm): Cumulative effective rainfall rate during the 120 minutes rainfall event, which equals the difference between total rainfall and total runoff.

$$I = \sum_{t=0}^{120} it = \sum_{t=0}^{120} rt - \sum_{t=0}^{120} qt \quad (3)$$

- Wetting front rate (v_{wf}, mm/min): The distance between moisture sensors 1 and 3 (or 2 and 4) (50 mm) divided by the time taken to travel from one to the other. The wetting front rate evaluates how fast the wetting front moved downward. The photographs from the side of flume were converted to black and white in order to show the infiltration modes. Six times were selected for each test to represent the evolution of the wetting fronts.

$$V_{wf} = \frac{50}{\Delta t} \quad (4)$$

The hydrological responses of the treated and untreated soils were sensitive to wettability changes, and thus the tests were analyzed in 3 categories according to the wettability, i.e. wettable soil, subcritical water repellent soil and water repellent soil. The effects of soil water repellency were compared among categories, while the influences of slope angle, RI and relative compaction were studied within each level. One representative test was selected from each group and presented in time series to describe the typical responses. The volumetric water content change, runoff and effective rainfall data are shown in Figure 6 to Figure 8, and the infiltration modes are summarized in Figure 9.

Statistical analysis is also conducted, the normality and homogeneity of all variables are verified using the Lilliefors test and Bartlett test, respectively. When the assumptions are satisfied, the parametric test (balanced one-way ANOVA) is used. If the null hypothesis is rejected, the non-parametric test (Kruskal-Wallis test) (Kruskal and Wallis, 1952) is then adopted.

3. Results

3.1. Calibration of moisture sensor

Soil-specific calibrations were conducted for wettable and subcritical water repellent soils, with the calibration equations presented in Figure 10. Calibration was not performed for the water repellent soil as infiltration did not occur. The calibration equation obtained for the wettable soil was VWC = $9 \times 10^{-4} \times$ raw - 0.4537, where VWC is the volumetric water content, and was different from the calibration equation provided by the manufacturer (VWC = $8.5 \times 10^{-4} \times$ raw - 0.48), which consistently provided lower volumetric water contents. The calibration equation for the subcritical water repellent soil was VWC = $4 \times 10^{-4} \times$ raw - 0.2156, suggesting that this relation is considerably affected by the DMDCS treatment. However, the calibration equation for the wettable soil was used for all tests, as will be discussed later.

3.2. Statistical analysis

The statistical significance analysis on the impacts of RI, slope angle, relative compaction and initial wettability are summarized in Table 4. The sample sizes, mean values, standard deviations and p-values (significance level = 0.05) are presented. From the analysis, the impacts of relative compaction and slope angle on all five measurements are not statistically significant. As for the effects of RI, time to ponding, time to steady state, wetting front rate and total water storage show statistical non-significance, whereas a strong correlation is observed between RI and runoff acceleration. The effect of the initial wettability on the hydrological responses is verified, as the results of various wettability are of different statistical significance.

The effects of RI, slope angle, relative compaction and initial wettability on hydrological responses are presented in Figure 11. Results of all tests are summarized together, box and whisker plots are adopted to establish comparisons among the data sets. In the plot, the ends of the box are the upper and lower quartiles, the median is marked by a solid line inside the box, and the mean is marked by a cross inside the box, the whiskers are the two lines outside the box that extend to the highest and lowest values observed.

3.3. Wettable soils

The results of representative wettable soil are shown in Figure 6 (test 1). The runoff rate and effective rainfall rate are presented in Figure 6a, the change in volumetric water content at several locations are recorded once a minute in Figure 6b, the infiltration mode is presented in Figure 9a. An expanding wetted zone at the slope toe was observed which was caused by the accumulation of water near the baffle. The remaining part of the slope was not affected. Figure 9a shows a wetting front parallel to the slope surface and moving downward gradually, this observation agreed with the results of volumetric water content change (Figure 6b) with the readings of sensor 1 and 2 unchanged at the beginning and suddenly rising at 7 minutes simultaneously. At 22 minutes, the same responses occurred for sensors 3 and 4. The time difference between sensors 1 and 2, and sensors 3 and 4 was 15 minutes. During infiltration, the volumetric water content kept increasing until 47.2% for moisture sensors 1 and 2. This implies the soil was nearly saturated, since for the soils at 70% and 90% relative compaction, the volumetric water content at saturation should be 55.4% and 46.8%, respectively. The difference among moisture sensors (around 8% for sensors 1 and 2 and 3 and 4) (Figure 6b) could be due to the density increase with depth, as higher relative compaction leads to a lower volumetric water content at saturation.

The hydrological response of the wettable soils followed a three-stage sequence, regardless of the slope angle, RI and relative compaction (Figure 6a). In the first 15 minutes all rainfall infiltrated and no surface runoff was observed, implying that the RI was smaller than the initial infiltration capacity, which is the maximum rate at which water can infiltrate into a given soil. From 15 minutes to 65 minutes, the effective rainfall rate started to decrease together with a concomitant increase in runoff rate. At 65 minutes, a steady state was reached with the effective rainfall rate reduced to zero and the runoff rate equal to the RI i.e. all rainfall was converted to runoff.

The mean time to ponding (t_p) and mean time to steady state (t_{ss}) do not show much differences. The mean runoff acceleration (a_q) shows that high RI leads to high runoff acceleration (126.7 mm/h^2), comparing to 64.6 mm/h^2 at low RI (Figure 11c). The mean wetting front rate (v_{wf}) shows that the wetting front traveled faster under high RI (2.9 mm/min) than under low RI (1.8 mm/min) (Figure 11d). The total water storage (*S*) results suggest an influence of the slope angle with the steeper slopes allowing a lower total water storage (38.4 mm) than the gentler slopes (42.6 mm) (Figure 11e).

3.4. Subcritical water repellent soils

The results of representative subcritical water repellent soil are shown in Figure 7 (test 8). The runoff rate and effective rainfall rate are presented in Figure 7a, change in volumetric water content at several locations are recorded in Figure 7b, the infiltration mode is presented in Figure 9b (The other infiltration mode of subcritical water repellent soil is shown in Figure 9c and discussed later). Infiltration still occurred in the subcritical water repellent soil, although the wetting front rate was significantly reduced. This observation agreed with the result of the volumetric water content change (Figure 7b), with the readings of sensors 1 and 2 unchanged at the start of the test and rising at around 10 minutes. At 80 minutes, the volumetric water content in sensors 3 and 4 started to increase. The time difference between sensors 3 and 4, and sensors 1 and 2 was around 70 minutes, which is longer than the difference for the wettable soil (around 15 minutes). As for the infiltration mode, unlike the wettable soil whose wetting front was parallel to the slope surface, preferential flow (fingering) and horizontal percolation were observed in subcritical water repellent soil. Along with the evolution of infiltration, the volumetric water content kept increasing until the maximum was reached. For the subcritical water repellent soil, the reading of the sensors was very high at

59.7%, as the volumetric water content of the saturated soil is only 46.8%. However, the time at which the sensor measured the increase in the volumetric water content was accurate and was used to calculate the wetting front rate. The calibration equation for the subcritical water repellent soil was not adopted to acquire water content data. Because the influence of DMDCS treatment gradually reduced with the draining of subsurface flow, the calibration equation of the subcritical water repellent soil could change with time. Therefore, the calibration equation for the wettable soil was used for all tests.

The hydrological response of the sub-critical water repellent soils also followed a three-stage sequence, regardless of the slope angle, RI and relative compaction (Figure 7a). Runoff was observed from 0 minutes (when the rainfall started), implying that the initial infiltration capacity after treatment is reduced and less than the RI. The runoff rate increased from 0 to 20 minutes. From 20 to 65 minutes, the runoff rate increased albeit with a smaller runoff acceleration (around 15% of the first stage). From 65 minutes, a steady state was reached with the effective rainfall rate reduced to zero and the runoff rate equal to the RI i.e. all rainfall was converted to runoff.

The mean time to ponding and mean time to steady state have similar magnitudes. The runoff acceleration showed that high RI leads to high runoff acceleration (67.6 mm/h^2), comparing to 28.2 mm/h^2 at low RI (Figure 11c). The wetting front rate varied considerably for both high RI (0.5-1.5 mm/min) and low RI (0-1.4 mm/min) (Figure 11d), and the variation is less than that of wettable soil, indicating that the influence of RI on wetting front rate was not as significant as soil water repellency. The total water storage, showed that at a high slope angle the mean total water storage is slightly less (16.9 mm) than that of a low slope angle (31.6 mm), suggesting that there is less water storage in steeper slopes (Figure 11e).

3.5. Water repellent soils

The results of representative water repellent soil are shown in Figure 8 (test 15). The runoff rate and effective rainfall rate are presented in Figure 8a, the change in the volumetric water content at several locations are recorded in Figure 8b, the infiltration mode is presented in Figure 9d. Infiltration was prevented by the soil water repellency for all the tests, with only a thin layer at the millimeter scale of the slope surface wetted. The wetting front rate was not calculated as no infiltration was observed. This observation agreed with the volumetric water content data (Figure 8b), with the sensors readings unchanged for all tests.

Runoff was observed from 0 minutes with no infiltration occurring. However, sub-surface flow parallels to the surface were noted in the upper 2-3 mm with water flowing to the bottom of the model and wetting the baffle area. These observations differed from those of Lourenço et al. (2015c) where industrial silica sand was used and runoff, erosion and rills developed on the model surface. This difference could be linked to the differences in the particle size and mineralogy, the erodibility of cohesionless clean sand is much greater than completely decomposed granite, whose clay fraction provides sufficient cohesion to prevent erosion in the current study. As such, the erosion and rills were observed only with silica sand.

Only two stages in the runoff generation process were identified in Figure 8a, runoff rate increased up to a steady state condition. The runoff rate started to increase at the start of the test, until the steady state was reached at 30 minutes. After which a steady state was reached with the effective rainfall rate reduced to zero and the runoff rate equal to the RI i.e. all rainfall was converted to runoff.

There is no significant difference observed between the mean time to ponding and mean time to steady state. The runoff acceleration shows variable runoff acceleration for high RI (101.4-332.4 mm/h^2) and low RI (33.9-342 mm/h^2) (Figure 11c), implying that the water repellent condition of the soil dominates runoff regardless of the RI. The wetting front rate cannot be determined by Eq. (4) since no water reached the sensors (Figure 11d). According to the visual observation and runoff data, no infiltration was allowed and therefore the wetting front rate was 0. The total water storage showed that at a high slope angle the mean total water storage is slightly less (6.4 mm) than that of a low slope angle (12.9 mm), suggesting that less water can be stored in steeper slopes (Figure 11e). However, the total water storage should be 0 mm. Sources of infiltration include (1) subsurface flow at the uppermost 2-3 mm depth of the soil and, (2) infiltration near the baffle area due to the accumulation of water from the subsurface flow and the wettable nature of the baffle (acting as a preferential infiltration interface) (Figure 12).

4. Discussion

4.1. *Effect of initial soil wettability*

The initial wettability condition had a profound effect on the hydrological response of the soils, as shown by the statistical analysis. All tests are summarized and compared to examine the influence of the initial wettability condition on the runoff hydrograph, wetting front rate, total water storage, time to ponding, time to steady state and runoff acceleration.

The runoff hydrographs of the soils (*i.e.* the shape of the runoff/effective rainfall rate in Figures 6a, 7a and 8a) are shown in Figure 13. Since the RI and runoff rate of each test differs, the RIs for all tests are normalized to 100%, and the runoff rates are normalized accordingly. In general, Figure 13 shows that with the increase of soil water repellency, infiltration is inhibited and runoff is promoted, with less time required to reach the steady state. Three stages can be distinguished for the wettable soil: infiltration, runoff generation and steady state; three stages are also observed for the subcritical water repellent soil: rapid generation of runoff, slow generation of runoff and steady state; two stages are observed for the water repellent soil: runoff generation and steady. The sequence of stages can be used to interpret field data whenever wettability is assumed to be an intervening factor, and could be implemented in models predicting runoff generation in slopes.

The time to ponding is also compared among the different wettability levels in Figure 11a. The time to ponding shows a decrease with an increase in soil water repellency, from 33.1 minutes for the wettable soil to 8.8 minutes for the subcritical water repellent soil and 2.5 minutes for the water repellent soil, suggesting that the infiltration capacity of the soils is reduced with an increase in soil water repellency. This impact of fire-induced water repellency on the time scale of ponding is consistent with the literature. For example, Zavala et al. (2009) compared the time to ponding values of unaffected soil and fire burned soil, which were ~24 minutes and ~4 minutes respectively. Ebel and Moody (2017) collected soil-hydraulic property data from literature review and conducted a meta-analysis to compare unaffected soil and fire-burned soil. The authors reported time to ponding values of tens of minutes for wettable soil and less than one minute for water repellent soil. Although sorptivity is not directly measured in this study, the influence of water repellency on it can be deduced. Since the shortened time to ponding is often attributed to the reduced sorptivity, and consistent changes are observed in this study and literature, it is reasonable to conclude that sorptivity decreases with synthetically induced water repellency. As pointed out by Hallett et al. (2004), sorptivity can be reduced to 50% by water repellency.

The time to steady state shows a different response with soil water repellency (Figure 11b). The subcritical water repellent soil has the longest time to steady state. From a wettable to a subcritical water repellent condition, the time to steady state increases from 77.5 minutes to 88.8 minutes, followed by a decrease to 36.9 minutes for the water repellent soil. A similar trend is observed for the runoff acceleration (Figure 11c) where the subcritical soil achieves the lowest runoff acceleration at 47.9 mm/h^2. The runoff acceleration decreased from 83.3

mm/h^2 for the wettable soil to 47.9 mm/h^2 for the subcritical water repellent soil, increasing again to 153.5 mm/h^2 for the water repellent soil.

Since the time to steady state reflects the duration of the infiltration process, it can be inferred that the longer duration attained by the subcritical water repellent soils is beneficial if they are to be deployed as a fill material, for instance, for man-made or infrastructure slopes. The potential applications of subcritical water repellent soils have been discussed recently (Zheng et al., 2017). Since extreme wettability conditions (wettable and strong water repellency) can cause either landslides or erosion, the optimal conditions that reduce slope instability can be established if subcritical water repellent soil could be deployed on sloping ground. The time-scales for the steady state are longer because of the delayed and prolonged infiltration process. This is further supported by the runoff acceleration, with the subcritical water repellent soil developing the lowest runoff acceleration. These two measurements are not documented in literature and therefore not directly comparable to the results obtained under field conditions, and may be adopted to find the so-called optimal conditions.

The wetting front rates of all tests are also shown in Figure 11d, indicating a delay in the wetting process with the increase of soil water repellency. Since infiltration was fully prevented by water repellency and no water content change was detected in water repellent soil, its wetting front rate is determined to be 0. The wetting front rate of subcritical water repellent soil (1.0 mm/min) is significantly reduced compared to the wettable soil (2.4 mm/min), which is the maximum wetting front rate among the three wettability levels. Fox et al. (2007) studied the effects of fire-induced water repellency on saturated hydraulic conductivity, which decreased by about 37% and 23% for the fine and coarse fractions, respectively. Comparable results were also obtained by Robichaud (2000), when water repellent conditions are present, the saturated hydraulic conductivity of soil reduced between 10% and 40% during the onset of simulated rainfall. However, Scott (2000) used an infiltrometer to determine the infiltration rate of water repellent soils, and reported that the results did not prove to be very useful, particularly in that they concentrated at the low end of infiltration rate and could not distinguish between degrees of stronger repellency. This indicates that the hydrological properties of severe or extreme water repellent soil are challenging to obtain through conventional methods.

The total water storage at the end of each test is presented in Figure 11e. The mean total water storage decreased with an increase in soil water repellency, from 41.9 mm for the wettable soil to 24.2 mm for the subcritical water repellent soil, until 9.3 mm for the water repellent soil.

Comparable trends albeit involving different processes can be found in the literature. Ebel et al. (2012) and Jordán et al. (2016) monitored the runoff generation immediately after a wildfire and prescribed fire, which revealed some soil water repellency. The post-wildfire ash layer was found to act as a hydrologic buffer to store water at the storm time scale of minutes and then release the water over a period of days. Although the mechanism is different, the roles of the ash layer and the subcritical water repellent soil in controlling runoff are comparable. The results discussed in this section were obtained under field condition and the soil water repellency was incurred by wildfire or prescribed fire, it is possible that the influences of other processes (removal of vegetation cover, surface sealing and pore clogging by ash) are also involved. While in this study, soil water repellency is induced synthetically and its impact is investigated in isolation.

4.2. Effects of rainfall intensity, slope angle and relative compaction

The RI, slope angle and relative compaction had a limited effect on the hydrological response of the soils as shown by the statistical analysis. However, Ebel and Moody (2017) argued for a need to separate statistical significance from practical hydrologic relevance. Therefore, observed effects or trends between RI, slope angle and relative compaction and the hydrological variables (e.g. time to ponding) is discussed. RI is related to the time to ponding, the time to steady state and the runoff acceleration. High RI leads to less time to ponding and a higher runoff acceleration. A higher wetting front rate (2.9 mm/min) is also linked to a high RI for the wettable soil (2.0 mm/min for low RI), while this effect is not observed for the subcritical water repellent soil. Ebel and Moody (2017) also reported for burned soil more ponding for 100 mm/h rainfall than 20 mm/h rainfall, which is consistent with this study. Dunne et al. (1991) pointed out that for some soils, the infiltration rate is negatively correlated with rainfall intensity because of the development of surface seals, while on soils which do not form seals, the infiltration rate increases with the rainfall intensity. This corresponds to the increased wetting front rate with the increase of rainfall intensity for wettable soil. The relation between water storage and rainfall intensity was investigated by Huang et al. (2013), the water storage after rainfall across the soil profile increased and then decreased as the rainfall intensity grew. This relation was not verified in this study due to the restriction of laboratory test, i.e. only limited amount of water can be stored in the soil.

The total water storage in the soil is closely related to the slope angle, with steeper slopes leading to a lower total water storage regardless of the wettability level. However, there are substantial disagreements among researchers regarding the impacts of slope angle on infiltration. Fox et al. (1997) reported that infiltration rate decreased with increasing slope angle, and the dominant influence of slope angle on infiltration rate resulted from changes in overland flow depth and surface storage. Chaplot and Le Bissonnais (2000) discovered that infiltration rate reduced with increasing slope gradient for a crusted interrill area. While Ribolzi et al. (2011) conducted field experiments and concluded that infiltration increases with increasing slope steepness, owing to the development of more permeable structural crusts on steeper slopes. Similar view was also shared by Janeau et al. (2003), stating that the steady final infiltration rate increased sharply with increasing slope angle.

The relative compaction showed little influence on the hydrological response of the soils. For the subcritical repellent and water repellent soils, the wetting front rate was reduced by ~40% and ~100% respectively, comparing to the wettable soil and irrespective of the relative compaction. This implies that the delay in the infiltration process in the subcritical and the water repellent soil remains effective without a close control of the dry density, which may translate into practical benefits when placing these materials in the field. However, relative compaction has been reported to influence hydrological properties of soil. Meek et al. (1992) observed that the infiltration rate and hydraulic conductivity decreased by 53% and 86% respectively, when bulk density was increased from 1.6 to 1.8 Mg/m^3. The contradictory results may result from different initial moisture conditions, in this study the air-dried soil is used whereas the results were obtained under field condition in the literature.

The combination of the RI, slope angle and relative compaction may also influence the development of the wetting front in the subcritical water repellent soil. The infiltration modes evolved from a parallel wetting front (Figure 9a) to preferential flow (Figure 9b) as the soil wettability changed from wettable to subcritical water repellent. However, due to the different slope angles and relative compactions, two infiltration modes were identified in the subcritical water repellent soil. One refers to preferential flow with horizontal and vertical fingering, showing distinctive wet patches in a dry soil matrix (Figure 9b). The other is an oblique wetting front that saturates from the toe towards the back of the model possibly due to a combination of a high slope angle and high relative compaction (Figure 9c), and together with the accumulation of water in the baffle area (a boundary effect).

The observed hydrological behavior of synthetic water repellent soils may have implications at the field-scale. For water repellent soils and if they are to be deployed in the stabilization of infrastructure slopes, the field behavior is likely to resemble the model tests where no infiltration is allowed and the response to rainfall is runoff dominated. However, at a catchment scale and in natural water repellent soils, the distribution of natural water repellent soils is known to be patchy implying that the total water storage may increase with the scale. For wettable and subcritical water repellent soils, the time to ponding, time to steady state, runoff acceleration and total water storage are scale-dependent and are likely to increase with the increasing catchment area. The effective rainfall rate does not depend on the scale and the observed hydrological patterns (as in Figure 13) can be expected at larger scales.

4.3. DMDCS treatment and capacitance probe

The high volumetric water content for the sub-critical water repellent soil may be explained through changes of the electrical conductivity. As observed by Kelleners et al. (2004), the volumetric water content measured by the EC-5 was higher for saline solutions. Thompson et al. (2007) also reported a 4% to 7.5% relative increase in the measured soil water content for every 1 dS/m increase in the electrical conductivity. HCl is a by-product of the reaction between the DMDCS and the OH groups of the soil particles surfaces which requires water for the reaction to complete. After treatment, a small amount of HCl may remain on the soil, resulting in an increased electrical conductivity when water infiltrates. With the continuous subsurface flow, the concentration of HCl reduces with time, with the EC-5 returning to normal at the end of the test (Figure 7b: sensor 1 and 2).

4.4. Experimental considerations

The raindrop velocity of the artificial rainfall was not measured and is expected to be smaller than the terminal velocity of natural rainfall, owing to the short falling height (~1.5m). This would result in a lower raindrop impact on soil minimizing the effects of rain splash erosion (Vaezi et al., 2017). The terminal velocity of natural raindrops usually ranges from ~2 m/s to ~9 m/s depending on their size (Gunn and Kinzer, 1949), and based on the drop size generated by the nozzle, the terminal velocity of natural raindrops with similar size as in this research is estimated to be around 7 m/s (Wang and Pruppacher, 1977).

The onset of wetting in all slope models was accurately captured by the moisture sensors. However, the capacitance probes used were influenced by the electrical conductivity, showing unrealistically high volumetric water content for the subcritical water repellent soils. Due to this, only the timing of the moisture change was used in the analysis. In the future, other types of dielectric sensors such as TDR should be used to obtain the volumetric water content, to avoid the influence of electrical conductivity when working with treated soil. In addition, the EC-5 is known for being sensitive to changes in bulk density, with the output increasing with the bulk density (Parsons and Bandaranayake, 2009).

The lower boundary of the slope model influenced the hydrological response of the soil. There was excessive infiltration near the baffle area due to the accumulation of water from the subsurface flow and due to the wettable nature of the baffle (acting as a preferential infiltration interface) (Figure 9). This response was included in the data analysis leading to an overestimation of the effective rainfall rate and total water storage. The thickness of the soil was only 10 cm and water was unable to drain out of the bottom of the flume. Then the subsurface flow had to drain out of the baffle, the runoff measured included both surface and subsurface runoff, and cannot be distinguished. This limitation in experimental setting needs to be considered in the future. Direct measurement of soil-hydraulic properties (e.g. saturated hydraulic conductivity, sorptivity etc.) should also be considered to allow comparison with other field and laboratory investigations.

Conclusion

Analysis of experimental data from a series of 24 flume tests in completely decomposed granite from Hong Kong at various soil water repellency levels, rainfall intensities, slope angles and relative compactions revealed that: (1) An increase in water repellency leads to a significant drop in both the wetting front rate (by ~40% and ~100% for the subcritical water repellent and water repellent soil, respectively) and the total water storage (by ~42% and ~77% for the subcritical water repellent and water repellent soil, respectively), (2) The time to ponding is shortened by an increase in water repellency (by ~74% and ~92% for the subcritical water repellent and water repellent soil, respectively), (3) The time to steady state is longest for the subcritical water repellent soils implying that the infiltration process is longer in duration than for the wettable and water repellent soils, (4) Different runoff hydrographs were identified with infiltration modes ranging from a parallel wetting front (wettable soils) to preferential flow and an oblique wetting front (for the subcritical water repellent soils, depending on the slope angle and relative compaction).

The effect of rainfall intensity on the slope hydrology contrasted with that of the relative compaction. The increased rainfall intensity leads to shorter times to ponding and to steady state, as well as a higher runoff acceleration but none of these parameters were sensitive to the relative compaction. This implies that the delaying effect of water repellency on infiltration remains effective without requiring precise control of the relative compaction. For the slope angle, the total water storage was the only sensitive parameter increasing with a decrease of the slope angle.

While the trends obtained and processes identified in this study can be extended to man-made slopes and natural catchments with water repellent soils, the tested conditions were not extreme and were not able to capture all the processes that lead to extreme field events such as post-wildfire debris flows. For instance, the rather finer nature of the soils and a maximum rainfall intensity only at 70 mm/h, inhibited the development of overland flow and erosion. Future work will define the threshold conditions for these processes to initiate. However, the current research highlights the interplay between soil wettability and rainfall intensity in slope hydrology and promotes our understanding of natural runoff generation when soil wettability is considered in isolation.

Acknowledgements

This research was supported by the Research Grants Council of Hong Kong, grants

17205915 and T22-603/15-N. The testing material was provided by the Drainage Services Department, Hong Kong Government. Laboratory assistance by Mr. N. C. Poon and Mr. Xu Dong is acknowledged. We thank the three anonymous reviewers whose comments helped improve and clarify this manuscript.

References

Ahn, S., Doerr, S. H., Douglas, P., Bryant, R., Hamlett, C. A. E., McHale, G., Newton, M. I., Shirtcliffe, N. J. (2013). Effects of hydrophobicity on splash erosion of model soil particles by a single water drop impact. Earth Surface Processes and Landforms, 38(11), 1225-1233.

Bachmann, J., Ellies, A., & Hartge, K. (2000). Development and application of a new sessile drop CA method to assess soil water repellency. Journal of Hydrology, 231, 66-75.

Bardet, J.-P., Jesmani, M., & Jabbari, N. (2014). Permeability and compressibility of wax-coated sands. Géotechnique, 64(5), 341-350.

Bisdom, E., Dekker, L., & Schoute, J. T. (1993). Water repellency of sieve fractions from sandy soils and relationships with organic material and soil structure. Geoderma, 56(1-4), 105-118.

BS 1377-3:1990, 1990. Methods of test for soils for civil engineering purposes. Chemical and electro-chemical tests. BSI, UK.

Cannon, S. H., Gartner, J. E., Wilson, R. C., Bowers, J. C., & Laber, J. L. (2008). Storm rainfall conditions for floods and debris flows from recently burned areas in southwestern Colorado and southern California. Geomorphology, 96(3-4), 250-269.

Chaplot, V., & Le Bissonnais, Y. (2000). Field measurements of interrill erosion under different slopes and plot sizes. Earth Surface Processes and Landforms, 25(2), 145-153.

Choi, Y., Choo, H., Yun, T., Lee, C., & Lee, W. (2016). Engineering Characteristics of Chemically Treated Water-Repellent Kaolin. Materials, 9(12), 978.

Cobos, D. R., & Chambers, C. (2010). Calibrating ECH2O soil moisture sensors. Application Note, Decagon Devices, Pullman, WA.

Czachor, H., Doerr, S., & Lichner, L. (2010). Water retention of repellent and subcritical repellent soils: New insights from model and experimental investigations. Journal of Hydrology, 380(1), 104-111.

DeBano, L. F. (1981). Water repellent soils: a state-of-the-art. USDA Forest Service General Technical Report PS W-46 (22p).

DeBano, L. (2000). Water repellency in soils: a historical overview. Journal of Hydrology, 231, 4-32.

Dell'Avanzi, E., Guizelini, A., da Silva, W., & Nocko, L. (2010). Potential use of induced soil-water repellency techniques to improve the performance of landfill's alternative final cover systems. Unsaturated soils. CRC Press, Boca Raton, FL, 461-466.

Diskin, M. H., & Nazimov, N. (1996). Ponding time and infiltration capacity variation during steady rainfall. Journal of Hydrology, 178(1–4), 369-380.

Doerr, S. H. (1998). On standardizing the 'water drop penetration time' and the 'molarity of an ethanol droplet' techniques to classify soil hydrophobicity: a case study using medium textured soils. Earth Surface Processes and Landforms, 23(7), 663-668.

Doerr, S. H., Shakesby, R. A., Blake, W. H., Chafer, C. J., Humphreys, G. S., & Wallbrink, P. J. (2006). Effects of differing wildfire severities on soil wettability and implications for hydrological response. Journal of Hydrology, 319(1-4), 295-311.

Drainage Services Department. (2013). Stormwater drainage manual: Planning, Design and Management, 4th Edition. Government of the Hong Kong Special Administrative Region, Hong Kong.

Dunne, T., Zhang, W., & Aubry, B. F. (1991). Effects of Rainfall, Vegetation, and Microtopography on Infiltration and Runoff. Water Resources Research, 27(9), 2271-2285.

Ebel, B. A., Moody, J. A., & Martin, D. A. (2012). Hydrologic conditions controlling runoff generation immediately after wildfire. Water Resources Research, 48(3). W03529.

Ebel, B. A., & Moody, J. A. (2017). Synthesis of soil-hydraulic properties and infiltration timescales in wildfire-affected soils. Hydrological Processes, 31(2), 324-340.

Eckersley, D. (1990). Instrumented laboratory flowslides. Géotechnique, 40(3), 489-502.

Fox, D. M., Bryan, R. B., & Price, A. G. (1997). The influence of slope angle on final infiltration rate for interrill conditions. Geoderma, 80(1), 181-194.

Fox, D. M., Darboux, F., & Carrega, P. (2007). Effects of wildfire-induced water repellency on soil aggregate stability, splash erosion, and saturated hydraulic conductivity for different size fractions. Hydrological Processes, 21(17), 2377-2384.

Gunn, R., & Kinzer, G. D. (1949). The teminal volocity of fall for water droplets in stagnant air. Journal of Meteorology, 6(4), 243-248.

Hallett, P. D., Nunan, N., Douglas, J. T., & Young, I. M. (2004). Millimeter-scale spatial variability in soil water sorptivity. Soil Science Society of America Journal, 68, 352–358.

Hamlett, C. A. E., Atherton, S., Shirtcliffe, N. J., McHale, G., Ahn, S., Doerr, S. H., Bryant, R., Newton, M. I. (2013). Transitions of water-drop impact behaviour on hydrophobic and hydrophilic particles. European Journal of Soil Science, 64(3), 324-333.

Huang, J., Wu, P., & Zhao, X. (2013). Effects of rainfall intensity, underlying surface and slope gradient on soil infiltration under simulated rainfall experiments. Catena, 104, 93-102.

Iverson, R. M., & LaHusen, R. G. (1993). Friction in debris flows: inferences from large-scale flume experiments. In American Society of Civil Engineers, Hydraulic Engineering ’93 Conference, San Francisco, California, July 25–30 1993, Proceedings, p. 1604–1609.

Janeau, J.L., Briquet, J.P., Planchon, O., Valentin, C. (2003). Soil crusting and infiltration on steep slopes in northern Thailand. European Journal of Soil Science, 54(3), 543–553.

Jordán, A., Zavala, L. M., Granged, A. J. P., Gordillo-Rivero, Á. J., García-Moreno, J., Pereira, P., . . . Alanís, N. (2016). Wettability of ash conditions splash erosion and runoff rates in the post-fire. Science of The Total Environment, 572, 1261-1268.

Kean, J. W., Staley, D. M., Leeper, R. J., Schmidt, K. M., & Gartner, J. E. (2012). A low-cost method to measure the timing of postwildfire flash floods and debris flows relative to rainfall. Water Resources Research, 48(5), W05516.

Kelleners, T. J., Soppe, R. W. O., Ayars, J. E., & Skaggs, T. H. (2004). Calibration of Capacitance Probe Sensors in a Saline Silty Clay Soil. Soil Science Society of America Journal, 68(3), 770-778.

Kruskal, W. H., & Wallis, W. A. (1952). Use of ranks in one-criterion variance analysis. Journal of the American Statistical Association, 47, 583–621.

Lee, C., Yang, H.-J., Yun, T. S., Choi, Y., & Yang, S. (2015). Water-Entry Pressure and Friction Angle in an Artificially Synthesized Water-Repellent Silty Soil. Vadose Zone Journal, 14(4).

Leelamanie, D., & Karube, J. (2009). Time dependence of CA and its relation to repellency persistence in hydrophobized sand. Soil Science and Plant Nutrition, 55(4), 457-461.

Li, P. W., & Lai, E. S. T. (2004). Short-range quantitative precipitation forecasting in Hong Kong. Journal of Hydrology, 288(1-2), 189-209.

Lourenço, S. D. N., Sassa, K., & Fukuoka, H. (2006). Failure process and hydrologic response of a two layer physical model: Implications for rainfall-induced landslides. Geomorphology, 73(1), 115-130.

Lourenço, S. D. N., Jones, N., Morley, C., Doerr, S. H., & Bryant, R. (2015a). Hysteresis in the Soil Water Retention of a Sand-Clay Mixture with CAs Lower than Ninety Degrees. Vadose Zone Journal, 14(7).

Lourenço, S., Woche, S., Bachmann, J., & Saulick, Y. (2015b). Wettability of crushed air-dried minerals. *Géotechnique Letters, 5*(3), 173-177.

Lourenço, S. D. N., Wang, G.-H., & Kamai, T. (2015c). Processes in model slopes made of mixtures of wettable and water repellent sand: Implications for the initiation of debris flows in dry slopes. Engineering Geology, 196, 47-58.

Lumb, P. (1965). The residual soils of Hong Kong. Géotechnique, 15(2), 180-194.

Meek, B. D., Rechel, E., Carter, L. M., DeTar, W. R., & Urie, A. (1992). Infiltration rate of a sandy loam soil: effects of traffic, tillage, and plant roots. Soil Science Society of America Journal, 56(3), 908-913.

Meyers, L., & Frasier, G. W. (1969). Creating hydrophobic soil for water harvesting. Journal of Irrigation and Drainage Engineering, 95, 43-54.

Ng, S. H. Y., & Lourenço, S. D. N. (2016). Conditions to induce water repellency in soils with dimethyldichlorosilane. Géotechnique, 66(5), 441-444.

Parsons, L. R., & Bandaranayake, W. M. (2009). Performance of a new capacitance soil moisture probe in a sandy soil. Soil Science Society of America Journal, 73(4), 1378-1385.

Ribolzi, O., Patin, J., Bresson, L. M., Latsachack, K. O., Mouche, E., Sengtaheuanghoung, O., . . . Valentin, C. (2011). Impact of slope gradient on soil surface features and infiltration on steep slopes in northern Laos. Geomorphology, 127(1), 53-63.

Ritsema, C. J., & Dekker, L. W. (2000). Preferential flow in water repellent sandy soils: principles and modeling implications. Journal of Hydrology, 231-232, 308-319.

Robichaud, P. R. (2000). Fire effects on infiltration rates after prescribed fire in Northern Rocky Mountain forests, USA. Journal of Hydrology, 231, 220-229.

Robichaud, P. R., Wagenbrenner, J. W., Pierson, F. B., Spaeth, K. E., Ashmun, L. E., & Moffet, C. A. (2016). Infiltration and interrill erosion rates after a wildfire in western Montana, USA. Catena, 142, 77-88.

Saulick, Y., Lourenço, S. D. N., & Baudet, B. A. (2017). A Semi-Automated Technique for Repeatable and Reproducible Contact Angle Measurements in Granular Materials using the Sessile Drop Method. Soil Science Society of America Journal, 81(2), 241-249.

Scott, D. F. (2000). Soil wettability in forested catchments in South Africa; as measured by different methods and as affected by vegetation cover and soil characteristics. Journal of Hydrology, 231, 87-104.

Stoof, C. R., Slingerland, E. C., Mol, W., Van Den Berg, J., Vermeulen, P. J., Ferreira, A. J. D., . . . Steenhuis, T. S. (2014). Preferential flow as a potential mechanism for fire-induced increase in streamflow. Water Resources Research, 50(2), 1840-1845.

Sun, H. W. (1999). Review of fill slope failures in Hong Kong. GEO Report No. 96. Geotechnical Engineering Office, Civil Engineering Department, 87 pp.

Thompson, R. B., Gallardo, M., Fernández, M. D., Valdez, L. C., & Martínez-Gaitán, C. (2007). Salinity Effects on Soil Moisture Measurement Made with a Capacitance Sensor. Soil Science Society of America Journal, 71(6), 1647-1657.

Tohari, A., Nishigaki, M., & Komatsu, M. (2007). Laboratory rainfall-induced slope failure with moisture content measurement. Journal of Geotechnical and Geoenvironmental Engineering, 133(5), 575-587.

Vaezi, A. R., Ahmadi, M., & Cerdà, A. (2017). Contribution of raindrop impact to the change of soil physical properties and water erosion under semi-arid rainfalls. Science of The Total Environment, 583, 382-392.

Wang, G., & Sassa, K. (2001). Factors affecting rainfallinduced flowslides in laboratory flume tests. Géotechnique, 51(7), 587-599.

Wang, P. K., & Pruppacher, H. R. (1977). Acceleration to Terminal Velocity of Cloud and Raindrops. Journal of Applied Meteorology, 16(3), 275-280.

Wijewardana, N. S., Kawamoto, K., Moldrup, P., Komatsu, T., Kurukulasuriya, L. C., & Priyankara, N. H. (2015). Characterization of water repellency for hydrophobized grains with different geometries and sizes. Environmental Earth Sciences, 74(7), 5525-5539.

Zavala, L. M., Jordán, A., Gil, J., Bellinfante, N., & Pain, C. (2009). Intact ash and charred litter reduces susceptibility to rain splash erosion post-wildfire. Earth Surface Processes and Landforms, 34, 1522 – 1532.

Zhang, H. Y., Zhu, S. B., Li, M., & Zhang, X. C. (2016). Water Repellency of Monument Soil

Treated by Tung Oil. Geotechnical and Geological Engineering, 34(1), 205-216.

Zheng, S., Lourenço, S. D. N., Cleall, P. J., Millis, S. W., Ng, A. K. Y., & Chui, T. F. M. (2017). Synthetic Water Repellent Soils for Slope Stabilization. In M. Mikoš, Ž. Arbanas, Y. Yin, & K. Sassa (Eds.), *Advancing Culture of Living with Landslides: Volume 3 Advances in Landslide Technology* (pp. 523-528). Cham: Springer International Publishing.

Captions of figures and tables

Table 1: Physical properties of Completely Decomposed Granite.

Table 2: Levels of water repellency and corresponding water drop penetration time. *After* Doerr (1998).

Table 3: Summary of flume tests.

Table 4: Statistical analysis on impacts of rainfall intensity, slope angle, relative compaction and initial wettability (significance level = 0.05).

Figure 1: Particle size distribution of CDG.

Figure 2. WDPT and CAs for CDG as percentage by soil mass of DMDCS.

Figure 3. CAs of CDG with time after treatment.

Figure 4. Configuration of flume model. (a) Schematic illustration of dimensions and instruments. (b) View of the flume installation.

Figure 5: Schematic for the variables used; runoff rate (q); effective rainfall rate (i); time to ponding (t_p); time to steady state (t_{ss}); runoff acceleration (a_q); total water storage (S).

Figure 6. Time series data for a flume test with wettable soil (test 1). (a) Runoff rate and effective rainfall rate. (b) Volumetric water content at various locations.

Figure 7. Time series data for a flume test with subcritical water repellent soil (test 8). (a) Runoff rate and effective rainfall rate. (b) Volumetric water content at various locations.

Figure 8. Time series data for a flume test with water repellent soil (test 15). (a) Runoff rate and effective rainfall rate. (b) Volumetric water content at various locations.

Figure 9. Photographs of the infiltration modes, black and white color denote wet and dry zones respectively, dotted red line indicates extent of wetting front (slope toes are at the left-hand side of photos, upper 9 cm of the slope shown). (a) Wettable soil (test 1). (b) Subcritical water repellent soil (test 11). (c) Subcritical water repellent soil (test 8). (d) Water repellent soil (test 3).

Figure 10. Calibration equations of EC-5 with wettable and subcritical water repellent soils.

Figure 11. Effects of rainfall intensity and slope angle on different soils. (a) Effect of rainfall intensity (RI) on time to ponding. (b) Effect of rainfall intensity (RI) on time to steady state. (c) Effect of rainfall intensity (RI) on runoff acceleration. (d) Effect of rainfall intensity (RI) on wetting front rate. (e) Effect of slope angle (SA) on total water storage.

Figure 12. Cross section near the slope toe after test: evidence of leak between the baffle and slope (test 3).

Figure 13. Runoff hydrographs of soils with various wettability (tests 8, 13, 15).

Tables and Figures

Table 1: Physical properties of Completely Decomposed Granite.

Parameters (unit)	Values
Specific gravity, G_s	2.65
Optimum water content	23%
Maximum dry density (g/cm^3)	1.57
Coefficient of uniformity, Cu	690
Coefficient of curvature, Cc	2.32
Maximum void ratio, e_{max}	1.37
Organic matter content	1.95%

Table 2: Levels of water repellency and corresponding water drop penetration time. *After* Doerr (1998).

Water repellency level	**WDPT (s)**
Wettable	⩽5 s
Slightly water repellent	5-60 s
Strongly water repellent	60-600 s
Severely water repellent	600-3600 s
Extremely water repellent	⩾3600 s

Table 3: Summary of flume test.

Test No.	Test settings					Test results				
	Initial volumetric water content (%)	CA (°)	Relative compaction (%)	Slope angle(°)	Rainfall intensity (mm/h)	Time to ponding (t_p, min)	Time to steady state (t_{ss}, min)	Runoff acceleration (a_q, mm/h^2)	Total water storage (*S*, mm)	Wetting front rate (v_{wf}, mm/min)
1	9.16	55	90	20	74.4±4.6	20	55	164.06	49.24	3.13
2	16.8	90				0	70	83.83	23.61	0.57
3	13.2	120				0	50	107.42	25.52	0.00
4	0.9	55	70			20	70	94.19	46.43	2.78
5	4.1	90				10	110	46.31	41.16	1.52
6	1.0	120				5	20	332.40	13.18	0.00
7	7.6	55	90	40	69.8±6.1	25	85	72.41	47.06	1.89
8	11.1	90				0	95	55.63	30.84	0.69
9	11.6	120				0	45	99.40	6.80	0.00
10	1.9	55	70			20	50	176.03	38.62	3.70
11	1.9	90				0	40	84.43	11.31	0.48

12	12.3	120				0	45	134.10	9.32	0.00
13	5.1	55	90	20	34.2±3.3	50	75	118.62	42.26	3.23
14	14.0	90				15	85	42.88	36.81	1.43
15	7.6	120				0	30	98.25	6.36	0.00
16	1.0	55	70			30	100	41.72	43.74	1.79
17	3.2	90				15	110	29.34	24.86	1.37
18	10.7	120				5	15	342.00	6.46	0.00
19	8.2	55	90	40	30.4±1.8	60	90	64.35	34.41	1.27
20	7.1	90				15	105	20.55	14.35	0.68
21	6.6	120				5	30	80.91	4.32	0.00
22	0.8	55	70			40	95	33.87	33.30	1.72
23	1.2	90				15	95	20.00	10.98	-
24	11.9	120				5	60	33.87	5.24	0.00

Table 4: Statistical analysis on impacts of rainfall intensity, slope angle, relative compaction and initial wettability (significance level = 0.05).

		Time to ponding		Time to steady state		Runoff acceleration		Wetting front rate		Total water storage	
Rainfall intensity	Values	30 mm/h	70 mm/h	30 mm/h	70 mm/h	30 mm/h	70 mm/h	30 mm/h	70 mm/h	30 mm/h	70 mm/h
	n=	12	12	12	12	12	12	12	12	12	12
	Mean	21.25	38.3	74.17	61.25	77.20	120.85	1.64	1.84	21.92	28.59
	Standard deviation	19.44	10.08	32.67	25.60	89.15	77.49	0.79	1.25	15.53	15.86
	p-value	0.0731		0.2927		0.0179		0.4775		0.3094	
Slope angle	Values	20°	40°	20°	40°	20°	40°	20°	40°	20°	40°
	n=	12	12	12	12	12	12	12	12	12	12
	Mean	14.17	15.42	65.83	69.58	125.08	72.96	1.32	0.87	29.97	20.55
	Standard deviation	14.75	18.76	32.88	26.92	106.33	46.94	1.24	1.13	15.47	15.13
	p-value	0.8577		0.7627		0.1841		0.3638		0.1489	
Relative compaction	Values	70%	90%	70%	90%	70%	90%	70%	90%	70%	90%
	n=	12	12	12	12	12	12	12	12	12	12

<table>
<tr><td rowspan="3"></td><td>Mean</td><td colspan="3">13.75</td><td colspan="3">15.83</td><td colspan="3">67.50</td><td colspan="3">67.92</td><td colspan="3">114.02</td><td colspan="3">84.03</td><td colspan="3">1.11</td><td colspan="3">1.07</td><td colspan="3">23.72</td><td colspan="3">26.80</td></tr>
<tr><td>Standard deviation</td><td colspan="3">12.27</td><td colspan="3">20.43</td><td colspan="3">34.15</td><td colspan="3">25.45</td><td colspan="3">114.36</td><td colspan="3">37.72</td><td colspan="3">1.25</td><td colspan="3">1.16</td><td colspan="3">15.98</td><td colspan="3">16.00</td></tr>
<tr><td>p-value</td><td colspan="6">0.7649</td><td colspan="6">0.9733</td><td colspan="6">0.7728</td><td colspan="6">0.9355</td><td colspan="6">0.6861</td></tr>
<tr><td rowspan="5">Contact angle</td><td>Values</td><td colspan="2">55°</td><td colspan="2">90°</td><td colspan="2">120°</td><td colspan="2">55°</td><td colspan="2">90°</td><td colspan="2">120°</td><td colspan="2">55°</td><td colspan="2">90°</td><td colspan="2">120°</td><td colspan="2">55°</td><td colspan="2">90°</td><td colspan="2">120°</td><td colspan="2">55°</td><td colspan="2">90°</td><td colspan="2">120°</td></tr>
<tr><td>n=</td><td colspan="2">8</td><td colspan="2">8</td><td colspan="2">8</td><td colspan="2">8</td><td colspan="2">8</td><td colspan="2">8</td><td colspan="2">8</td><td colspan="2">8</td><td colspan="2">8</td><td colspan="2">8</td><td colspan="2">8</td><td colspan="2">8</td><td colspan="2">8</td><td colspan="2">8</td><td colspan="2">8</td></tr>
<tr><td>Mean</td><td colspan="2">33.13</td><td colspan="2">8.75</td><td colspan="2">2.50</td><td colspan="2">77.50</td><td colspan="2">88.75</td><td colspan="2">36.88</td><td colspan="2">95.66</td><td colspan="2">47.87</td><td colspan="2">153.54</td><td colspan="2">2.44</td><td colspan="2">0.84</td><td colspan="2">0.00</td><td colspan="2">41.88</td><td colspan="2">24.24</td><td colspan="2">9.65</td></tr>
<tr><td>Standard deviation</td><td colspan="2">15.34</td><td colspan="2">7.44</td><td colspan="2">2.67</td><td colspan="2">18.32</td><td colspan="2">23.87</td><td colspan="2">15.57</td><td colspan="2">53.34</td><td colspan="2">25.59</td><td colspan="2">116.86</td><td colspan="2">0.88</td><td colspan="2">0.54</td><td colspan="2">0.00</td><td colspan="2">5.92</td><td colspan="2">11.52</td><td colspan="2">6.98</td></tr>
<tr><td>p-value</td><td colspan="6">0.0002</td><td colspan="6">7.126e-05</td><td colspan="6">0.0204</td><td colspan="6">0.0014</td><td colspan="6">9.427e-07</td></tr>
</table>

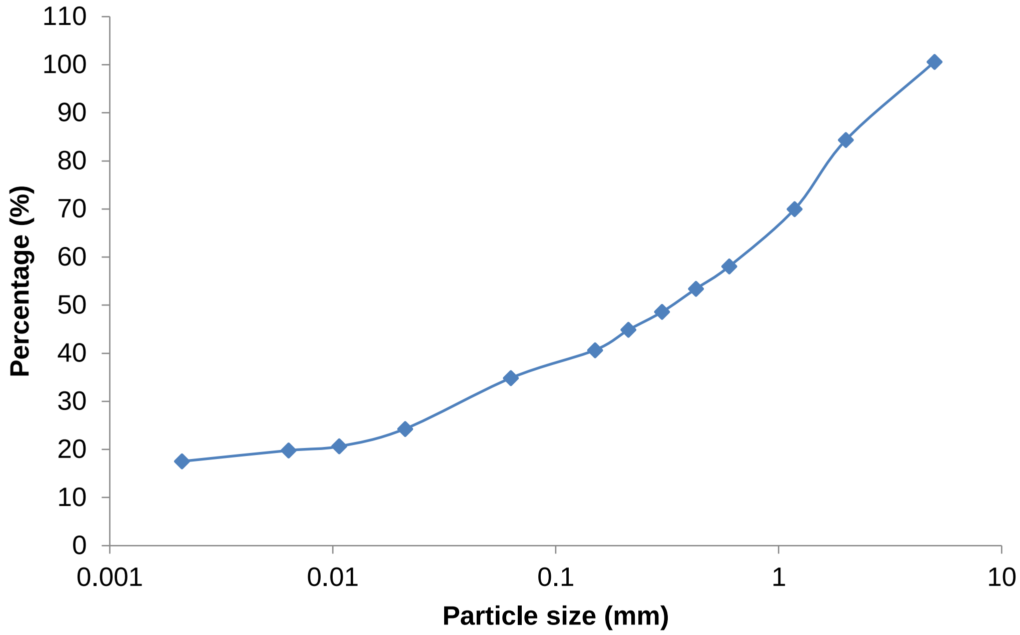

Figure 1: Particle size distribution of CDG.

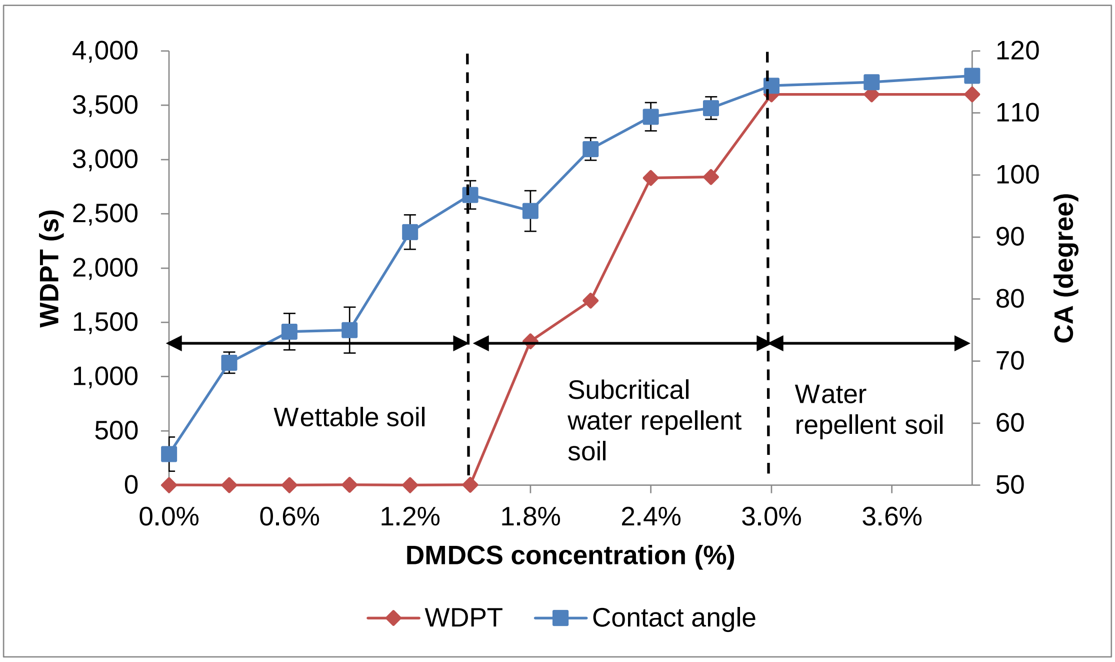

Figure 2. WDPT and CAs for CDG as percentage by soil mass of DMDCS.

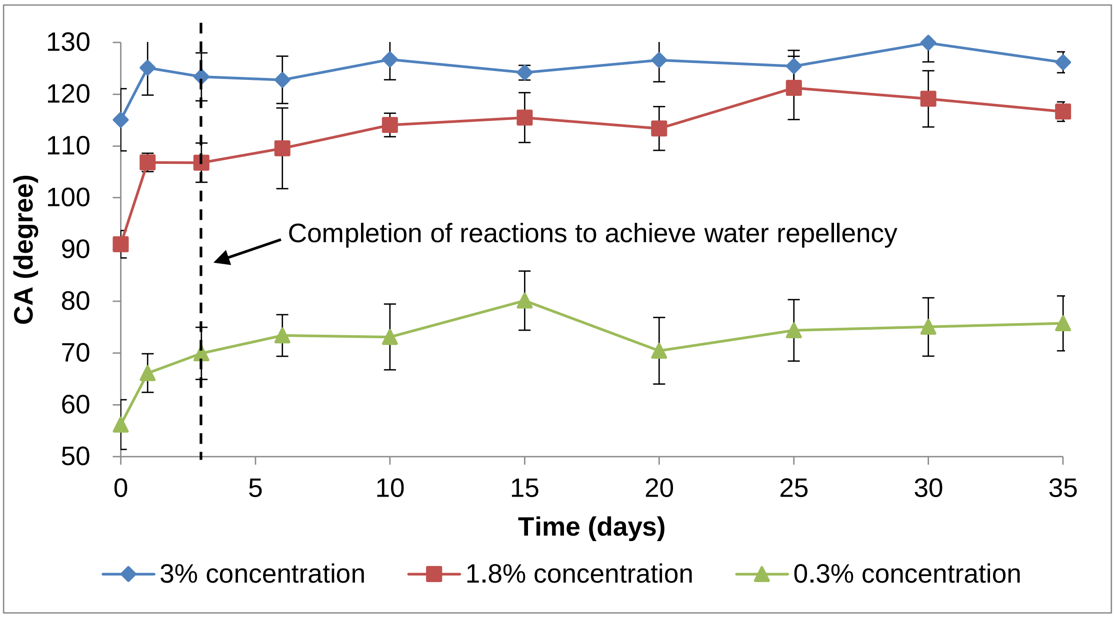

Figure 3. CAs of CDG with time after treatment.

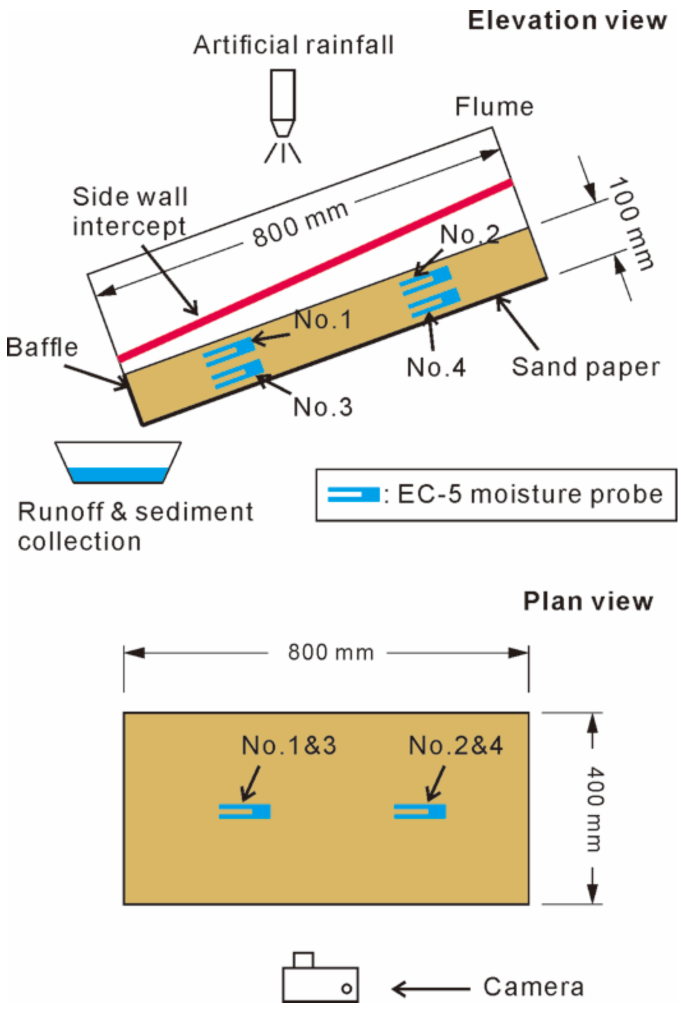

a

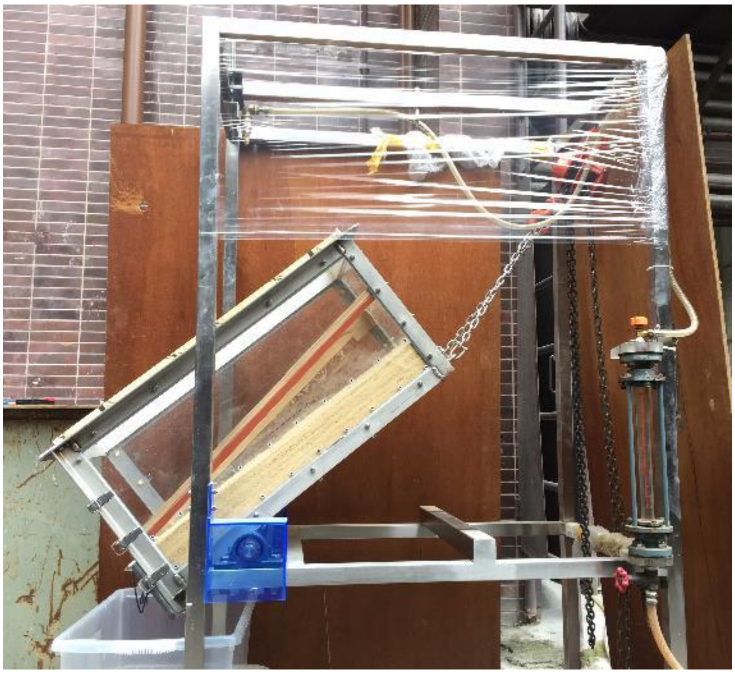

b

Figure 4. Configuration of flume model. (a) Schematic illustration of dimensions and instruments. (b) View of the flume installation.

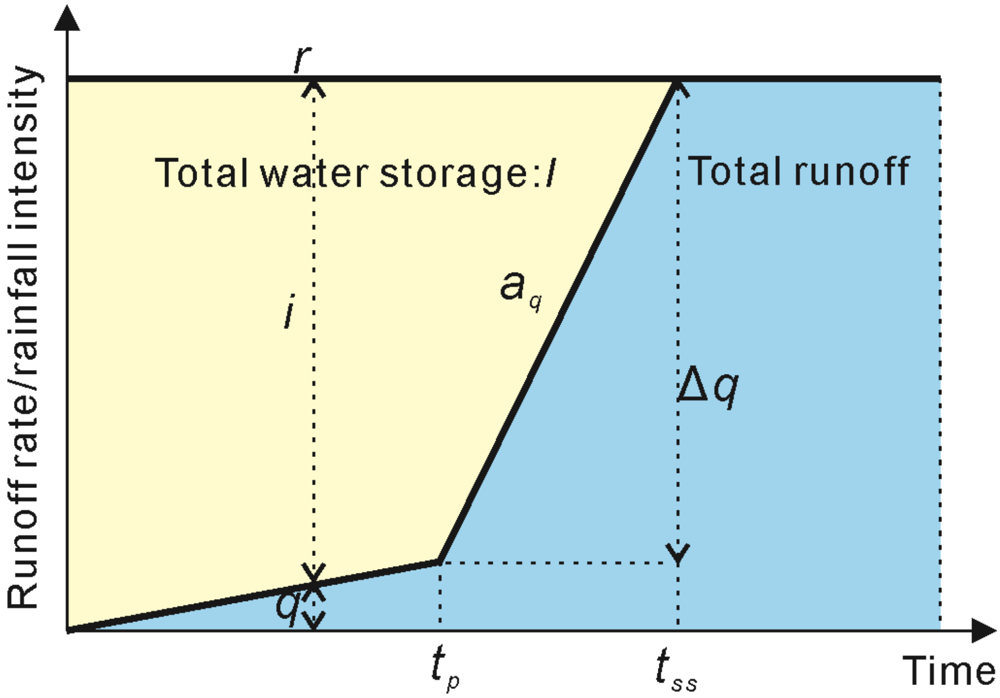

Figure 5: Schematic for the variables used; runoff rate (q); effective rainfall rate (i); time to ponding (t_p); time to steady state (t_{ss}); runoff acceleration (a_q); total water storage (S).

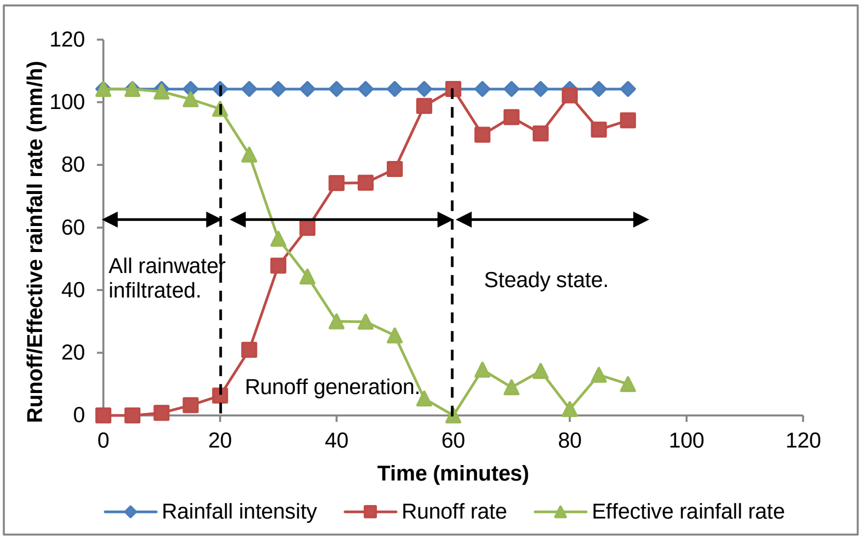

a

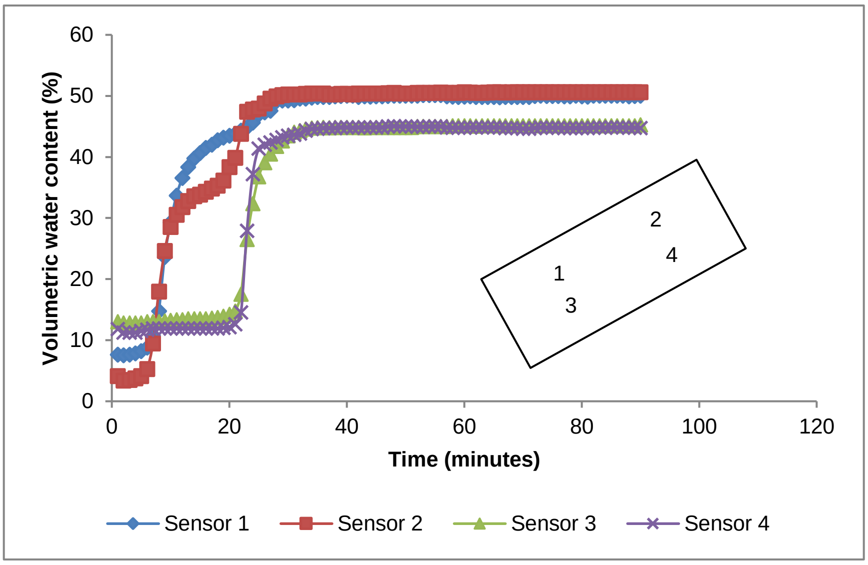

b

Figure 6. Time series data for a flume test with wettable soil (test 1). (a) Runoff rate and effective rainfall rate. (b) Volumetric water content at various locations.

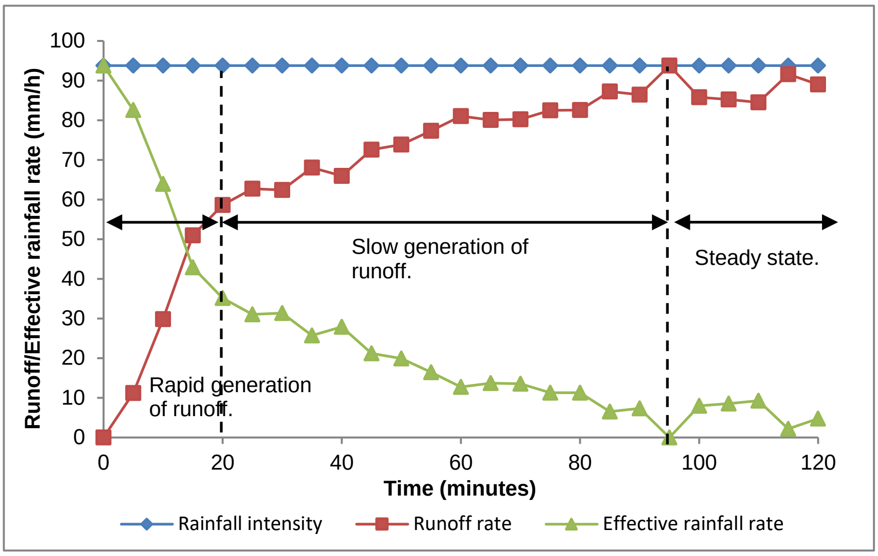

a

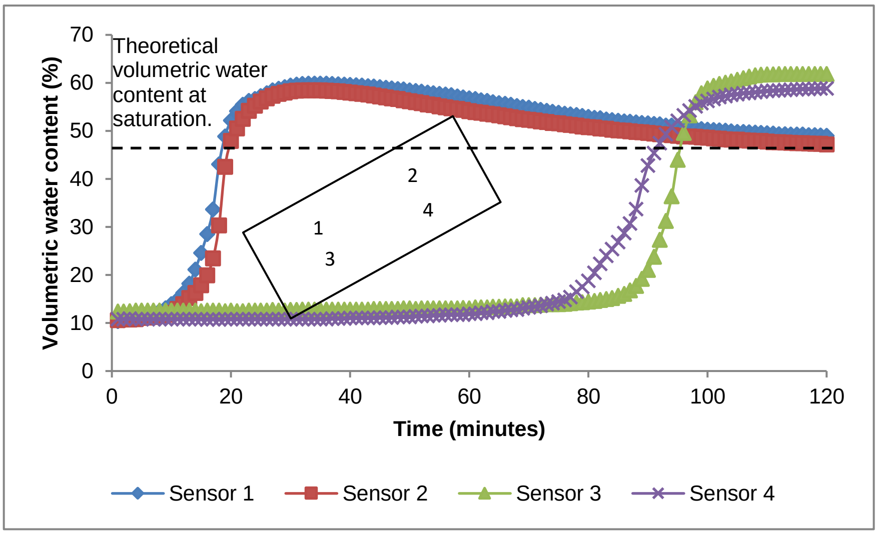

b

Figure 7. Time series data for a flume test with subcritical water repellent soil (test 8). (a) Runoff rate and effective rainfall rate. (b) Volumetric water content at various locations.

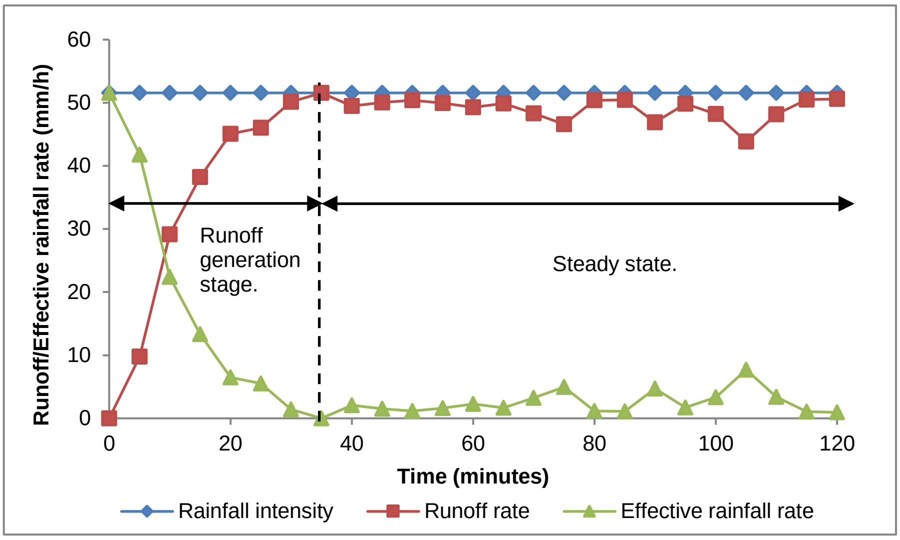

a

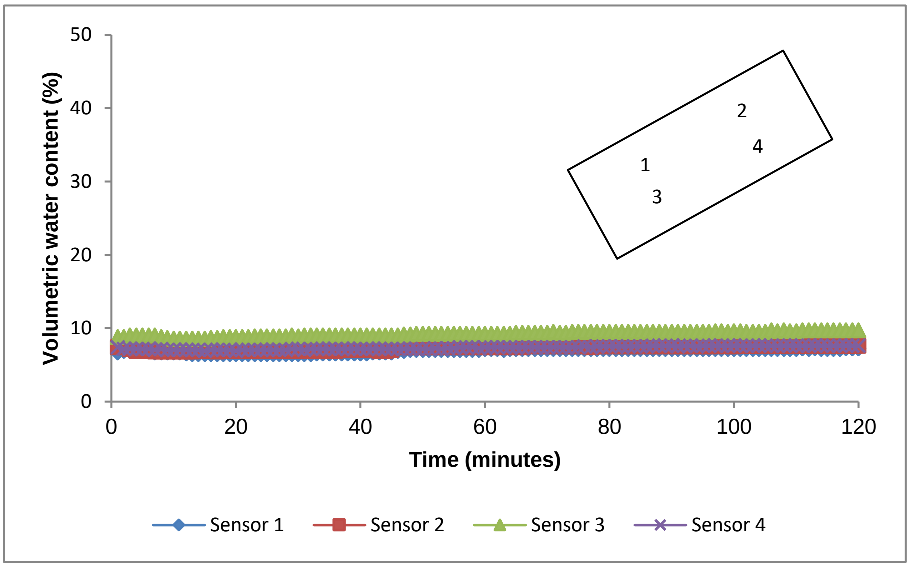

b

Figure 8. Time series data for a flume test with water repellent soil (test 15). (a) Runoff rate and effective rainfall rate. (b) Volumetric water content at various locations.

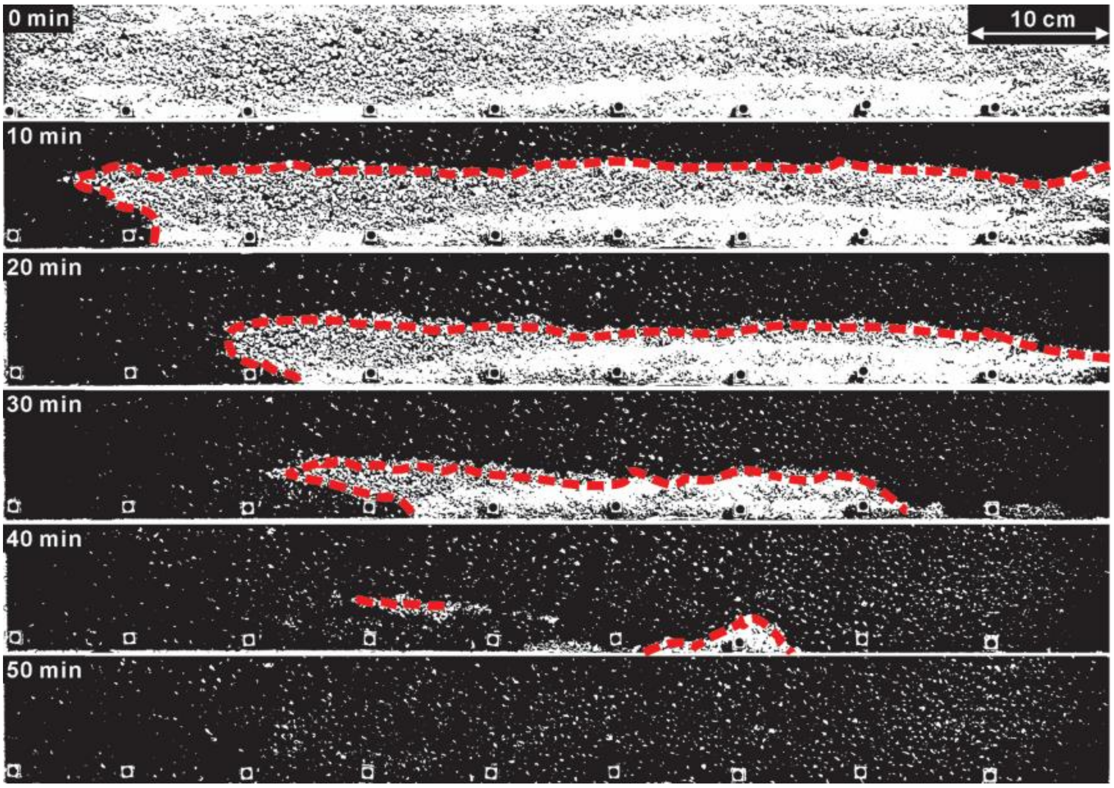
0 min
10 cm
10 min
20 min
30 min
40 min
50 min

a

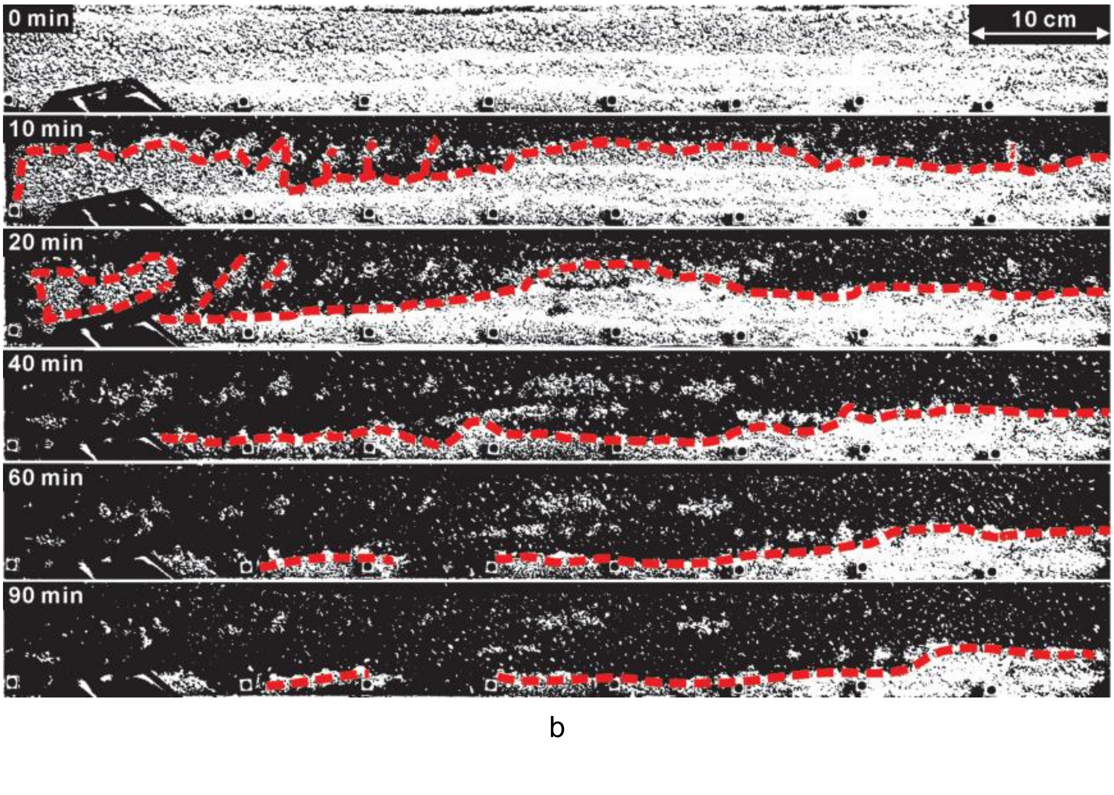
0 min
10 cm
10 min
20 min
40 min
60 min
90 min

b

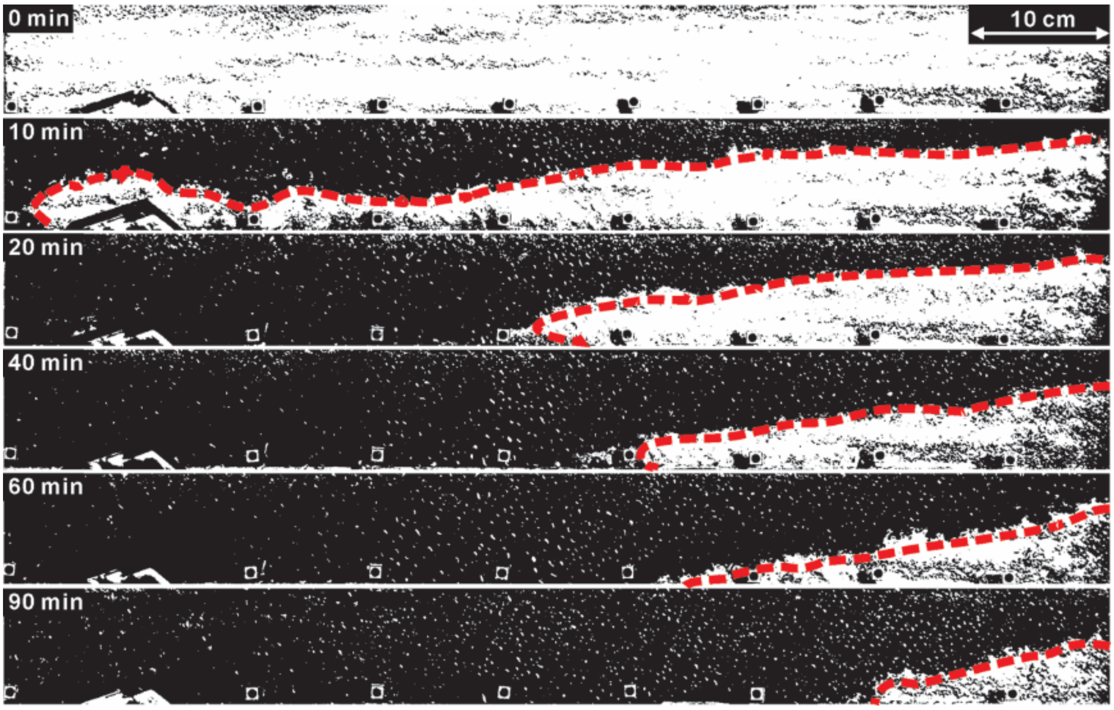

c

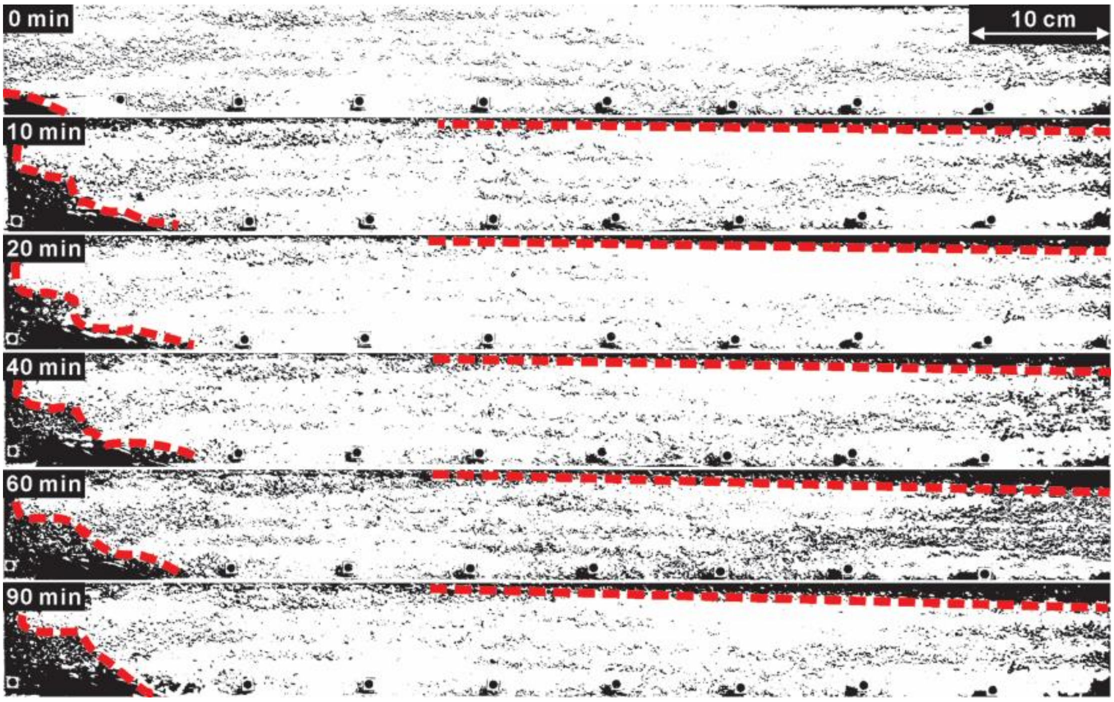

d

Figure 9. Photographs of the infiltration modes, black and white color denote wet and dry zones respectively, dotted red line indicates extent of wetting front (slope toes are at the left-hand side of photos, upper 9 cm of the slope shown). (a) Wettable soil (test 1). (b) Subcritical water repellent soil (test 11). (c) Subcritical water repellent soil (test 8). (d) Water repellent soil (test 3).

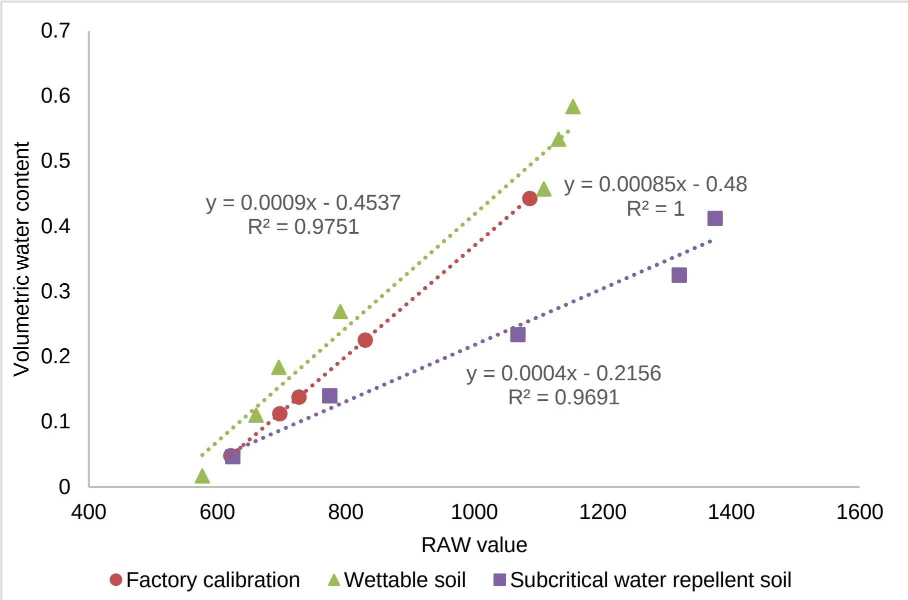

Figure 10: Calibration equations of EC-5 with wettable and subcritical water repellent soils.

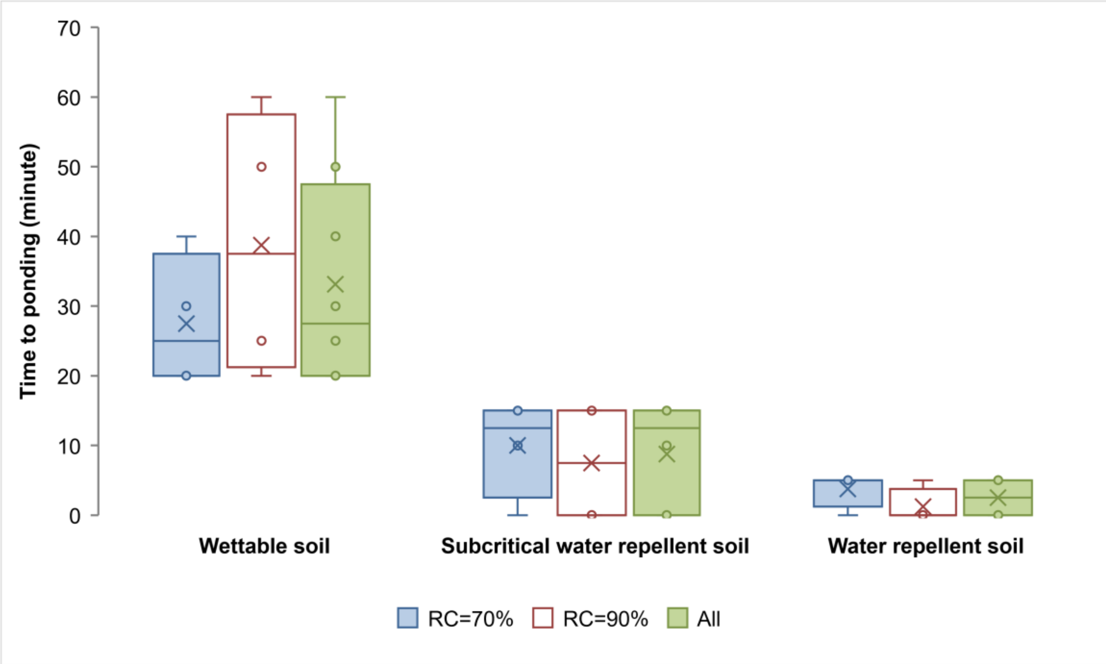

Time to ponding (minute)
70
60
50
40
30
20
10
0
Wettable soil
Subcritical water repellent soil
Water repellent soil
RC=70%
RC=90%
All

a

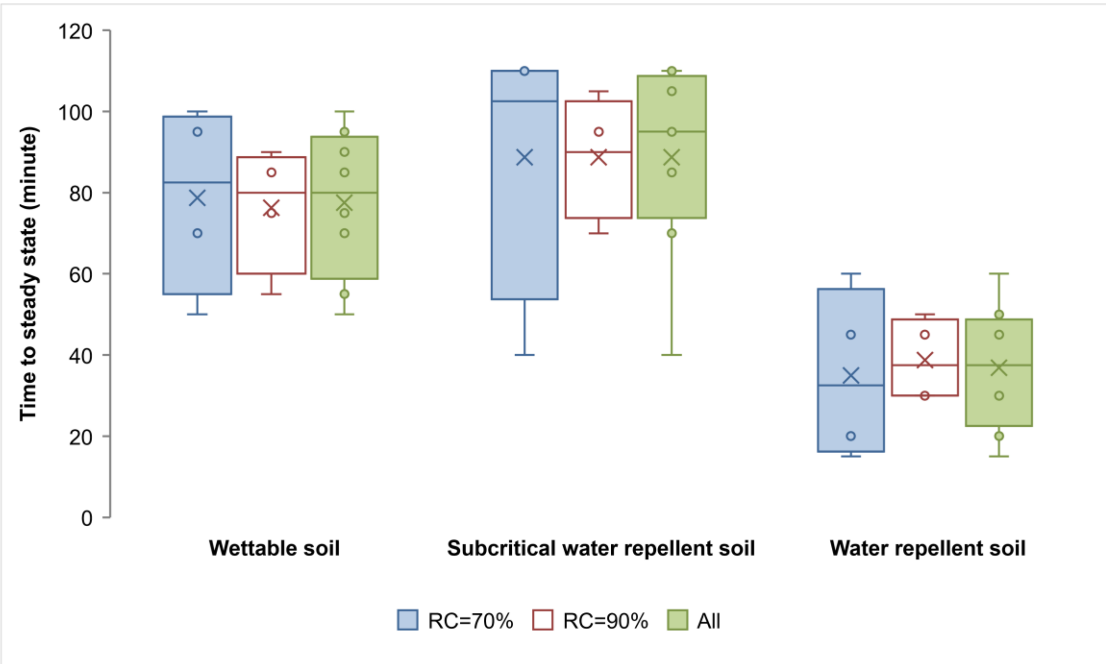

Time to steady state (minute)
120
100
80
60
40
20
0
Wettable soil
Subcritical water repellent soil
Water repellent soil
RC=70%
RC=90%
All

b

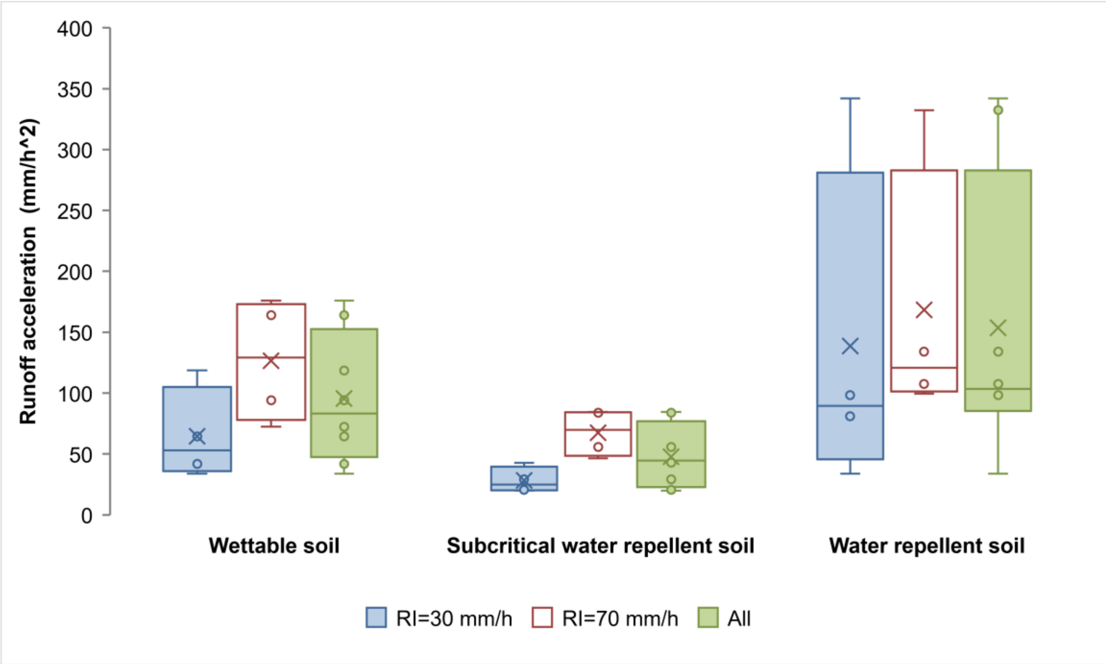
Runoff acceleration (mm/h^2)
400
350
300
250
200
150
100
50
0
Wettable soil
Subcritical water repellent soil
Water repellent soil
RI=30 mm/h
RI=70 mm/h
All

c

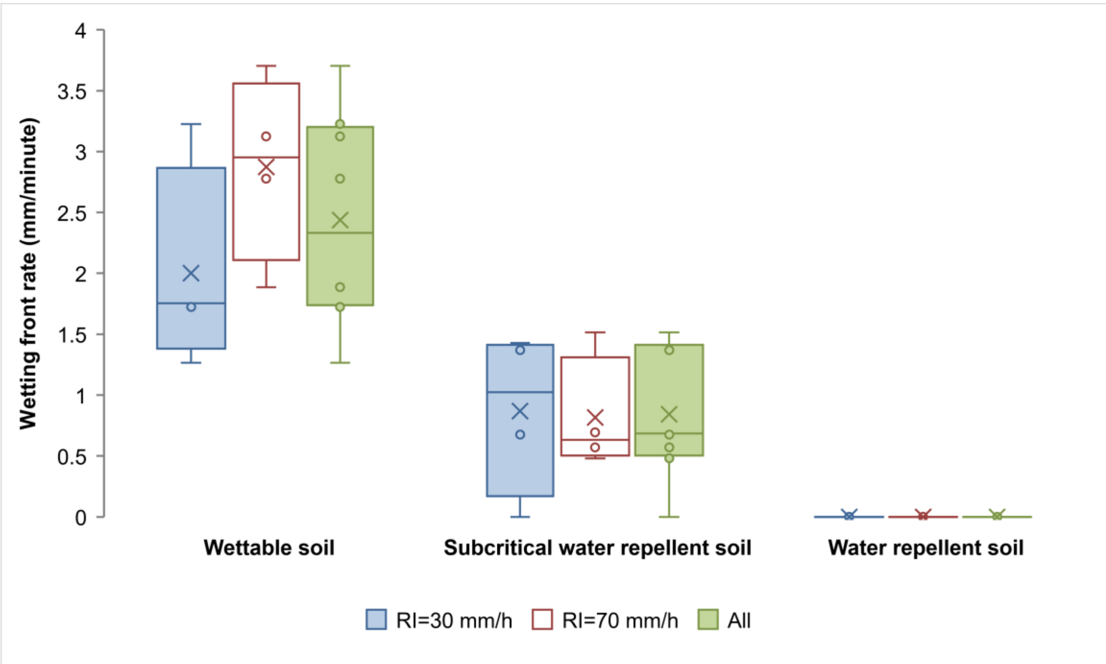
Wetting front rate (mm/minute)
4
3.5
3
2.5
2
1.5
1
0.5
0
Wettable soil
Subcritical water repellent soil
Water repellent soil
RI=30 mm/h
RI=70 mm/h
All

d

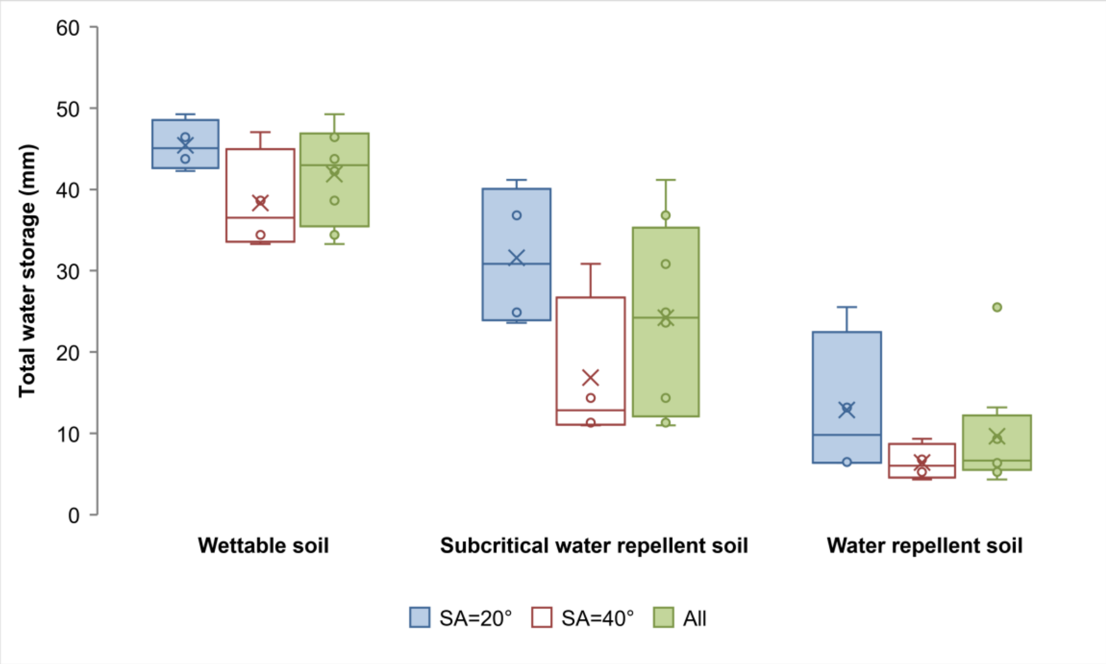

e

Figure 11. Effects of rainfall intensity and slope angle on different soils. (a) Effect of rainfall intensity (RI) on time to ponding. (b) Effect of rainfall intensity (RI) on time to steady state. (c) Effect of rainfall intensity (RI) on runoff acceleration. (d) Effect of rainfall intensity (RI) on wetting front rate. (e) Effect of slope angle (SA) on total water storage.

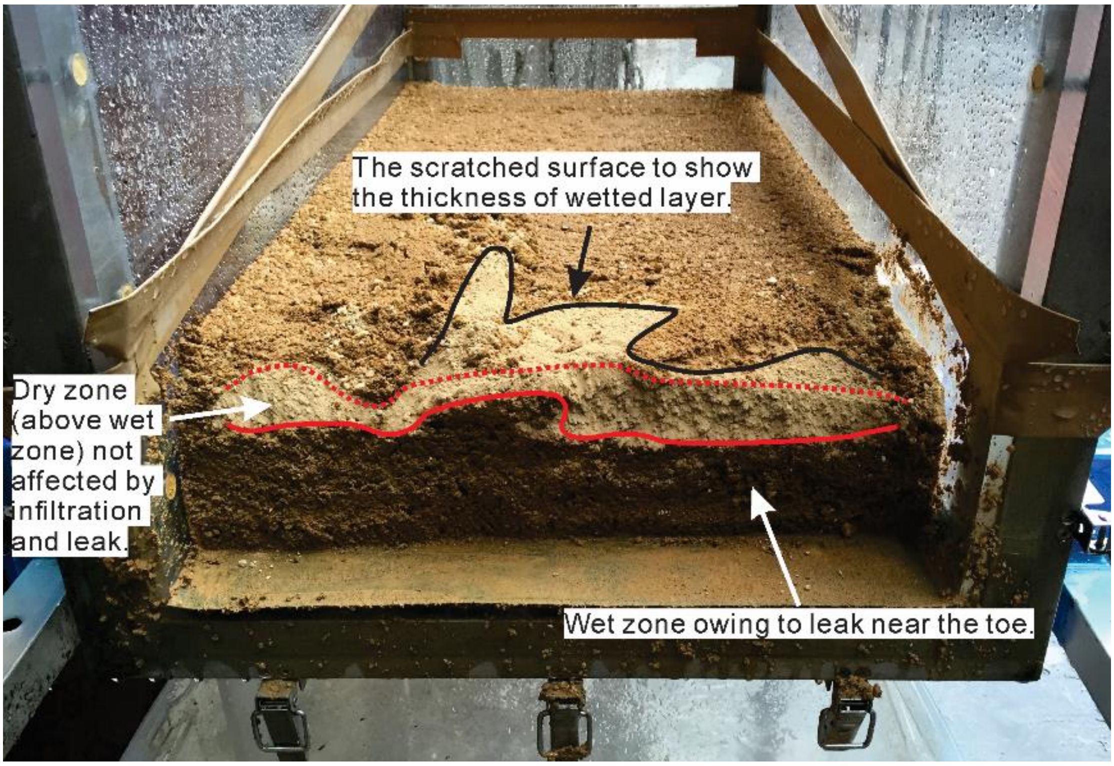

Figure 12. Cross section near the slope toe after test: evidence of leak between the baffle and slope (test 3).

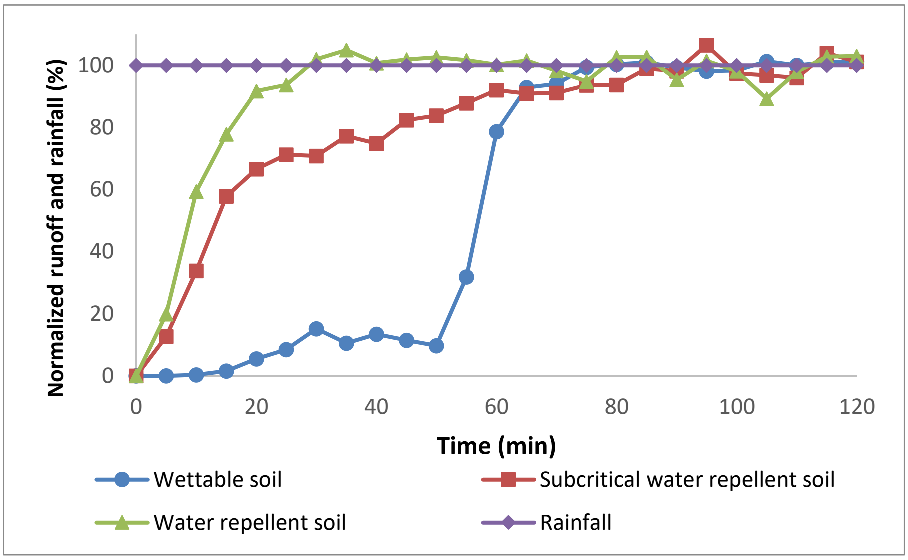

Figure 13. Runoff hydrographs of soils with various wettability (tests 8, 13, 15).